COSMIC RAY GROUP

School of Physics and Astronomy

UNIVERSITY OF MINNESOTA

In the Figure Section, change Figure 3 to Figure 4 and Figure 4 to Figure 3.

Page 7, line 17. Change (August 18) to (August 12).

Page 20, second line from the bottom. the closing bracket,), does not belong there.

George K. Parks

School of Physics and Astronomy, University of Minnesota
Minneapolis, Minnesota

Abstract

It is shown that the time profiles of trapped Van Allen electrons measured at synchronous altitudes and precipitated fluxes measured in the auroral zone are extremely well correlated. The freshly accelerated equatorial electrons are predominant in the 50-150 keV energies but when observed in 150-500 keV energies, they show different behavior. Equatorial electrons are created at all pitches but the pitch-angle distribution is peaked at 90°. The anisotropy in pitch-angle distribution increases and decreases with increasing and decreasing electron fluxes. Lifetime calculations from these simultaneous measurements show that typically, electrons during substorms have typical lifetimes of $\approx 10^3$ seconds, but some events have lifetimes as short as ≈ 200 seconds. The similarity of time profiles in precipitation and trapped fluxes, the differing behavior of ≈ 50 and 150 keV electrons, the flat pitch-angle distribution, and the behavior of anisotropy are consistent with strong pitch-angle diffusion model of Kennel (1969).

1. Introduction

One of the most fundamental problems in magnetospheric physics is the origin of the Van Allen energetic particles. Since about 1962, Winckler et al. (1962) recognized from observations that the outer zone magnetosphere would be completely exhausted of its energetic particles by the frequent auroral precipitation unless local acceleration mechanisms existed within the magnetosphere which could replenish the outer zones with freshly accelerated particles. To date, however, the magnetospheric acceleration or precipitation mechanisms are not completely known. Extensive observations of outer zone fluxes (see, for example, Frank (1965)) and of auroral precipitation (see O'Brien (1964)) are available. These observations, however, were not adequate to establish the precise relationship between outer zone flux variations and auroral precipitation nor could they establish in an unambiguous way whether the measured variations were due to spatial or temporal changes. Therefore, the early observations, although they provided information on the gross nature of the outer zone radiation, lacked the finer details needed to study the complicated wave-particle interactions and plasma instabilities responsible for particle acceleration and precipitation. This article presents detailed results of a particle correlation experiment conducted between the equatorial plane of the magnetosphere at synchronous altitudes and the magnetic conjugate in the auroral zone. These measurements differ from those in the past in that the outer zone electron fluxes are measured on board a geostationary platform (ATS-1) anchored at $6.6\ R_e$ equator. Since the satellite is fixed with respect to a point on the earth's surface, and since local magnetic field variations are also recorded, one can now distinguish spatial variations from temporal variations. Consequently, it

is now possible to distinguish flux variations recorded by the satellite
due to L-shell motion passing the satellite from true time variations
occurring on a given L-shell due to, for example, some magnetospheric
acceleration process. The measurements in the auroral zone are bremsstrahlung
X-rays from precipitated energetic electrons detected by means of high
altitude balloons.

After a short instrumentation section, we will present in Section 3
data from simultaneous particle observations of outer zone trapped fluxes
and the auroral precipitated fluxes during magnetospheric substorms.
In Section 4 the energy dependence of the accelerated particles is studied
at the equator during substorms, the precipitation electron energy spectrum
is derived, and lifetimes of these particles are calculated. In Section 5
we will study the pitch-angle distributions of the equatorial particles and
also study the behavior of the pitch-angle anisotropy as a function of
substorm time. In Section 6 we summarize the main features of the results
and qualitatively examine the various existing acceleration and precipitation
theories to explain our findings. (The question of particle modulation
or of ≃10 keV electrons associated with visual auroras are not treated in
this paper. A separate paper will study particle modulation phenomena.)
Some of the results shown in this paper were discussed in the 29th and
30th American Geophysical Union Meetings. Previous correlation studies of
outer Van Allen radiation and the auroral precipitation are contained in
Parks et al. (1968b); Parks and Winckler (1968, 1969).

2. Instrumentation

The detailed description of instrumentation on ATS-1 and auroral zone
balloons are given in Lezniak et al. (1968) and Parks and Winckler (1969).
It suffices to point out here that electron fluxes measured in the equatorial

plane are in the energy ranges 50-150 keV, 150-500 keV and 500-1000 keV.

In the text, ATS-1 particle rates are given in both units of counts/sample

and directional flux in $(cm^2\text{-sec-ster-keV})^{-1}$. The conversion factor from

counts/sample to flux in $(cm^2\text{-sec-ster-keV})^{-1}$ for the 50-150 keV is

4.5×10^2; for 150-500 keV, the factor is 7.79×10^1 and for the 500-1000 keV,

the factor is 4.0×10^1. The pitch-angles of these electrons, as will be

shown in detail (Section 5), are nominally between 60-90°. The satellite

is situated on the geographic equatorial plane ≈6.6 earth radii from the

center of the earth above Hawaii at ≈128° W geographic longitude, and the

satellite magnetic lines of force terminate in the auroral zone at

≈62.8° N latitude using the geomagnetic field model of Cain et al. (1964).

The high-altitude balloons were flown from College, Alaska

(62.4 N latitude and 150 W longitude) approximately 650 km west of the

ATS-1 conjugate. For the April 1967 series, the high altitude wind was

westerly. Consequently, most of bremsstrahlung measurements occurred to

the west of College, Alaska, separating the balloon and the ATS-1 field

line by more than 1300 km. The high altitude winds during the August 1967

series were calm and therefore data of bremsstrahlung come predominantly

from a region near College, Alaska. The X-ray energies detected were

above 20 keV and the balloon depths were usually at 2.3 gms/cm^2. Exceptions

to this rule will be indicated when appropriate. The hv > 20 keV corresponds

to most probable parent electron energies of about 40-50 keV if an

exponential electron energy spectrum is assumed with an e-folding energy

of about 20 keV (Section 4). Consequently, the electrons measured in the

auroral zone (precipitation) and the equator (trapped) are of similar

energies. The geometry factor of the balloon detector was ≈35 cm^2-ster,

and the detector assembly was NaI (Tl) crystals coupled to photomultiplier

tubes.

3. Correlation of Electron Fluxes Between Synchronous Altitudes

and the Auroral Zone

On a number of high-altitude balloon flights made from College, Alaska

(located approximately 660 km west of the ATS-1 satellite magnetic conjugate),

intense atmospheric bremsstrahlung X-rays from auroral precipitation of

energetic electron fluxes were detected during substorms. These measurements

have now been compared with the behavior of outer zone trapped radiation

detected at synchronous altitudes, and the results are presented below.

The main objective of this section is to show that intense auroral precipitation

does not occur randomly, but only during periods when large increases of

outer zone electron fluxes are encountered. It is emphasized that the

measurements taken in the equatorial plane represent trapped Van Allen

particles (see Section 5) since the pitch angles of these ATS-1 electrons

are large and therefore their mirror points lie close to the equatorial

plane of the magnetosphere. On the other hand, the precipitated particles

in the auroral zone, if traced along the field line to the equatorial

plane by using the adiabatic invarient, $\frac{\sin^2\alpha}{B}$ = const, have very small

equatorial pitch angles (a cone of less than 5°). The comparison is

therefore between particles that have very small equatorial pitch angles

($\approx 3°$) and those with pitch-angles that are predominantly between 60-90°.

A. Simultaneous ATS-1 and Auroral Observations.

In Figures 1 to 4 are shown the simultaneously observed auroral

X-ray count-rates and equatorial electron fluxes of energies 50-150 keV,

plotted as a function of time. With the exception of Figure 1, where the

count-rates represent 5 minute averages, the satellite and the balloon

X-ray data represent counts averaged over 1 minute. Again, with the

exception of the events displayed in Figure 1, the balloon data were

obtained at atmospheric depths of 2-3 gms/cm^2. The balloon depth for the events shown in Figure 1 was about 6 gms/cm^2.

Because the balloon reached the ceiling altitude at about 1500 UT (Figure 1) while an event was in progress (as can be inferred from equatorial electron flux-time profile), count-rate information prior to 1500 UT for X-rays is not available. Note however that the two time profiles of the event that occurred between 1505 and 1555 UT are well correlated. Similarly, the events that started around 1950 UT are also well correlated. The gap in the balloon data in the time interval 2015-2040 UT was due to telemetry fade out while the balloon was near the horizon, approximately 1000 km west of College, Alaska; some unusable data were recovered for about 15 minutes after 2040 UT during the decline of the event. The peak electron fluxes observed at the geostationary orbit in the energy interval 50-150 keV for the two events were about 6 and 8 x 10^4 (cm^2-sec-ster-keV)$^{-1}$, respectively. These were superposed on the ambient unstructured Van Allen fluxes of about 2 x 10^4 (cm^2-sec-ster-keV)$^{-1}$. Thus, the increases observed at peaks were larger than the ambient flux values by factors of 3 and 4. The X-ray peak flux at the balloon depth for $h\nu$ > 20 keV was about 300 (cm^2-sec)$^{-1}$ where the flux was averaged over the upper hemisphere. To obtain absolute electron fluxes that produced the observed bremsstrahlung intensity, it requires thick-target bremsstrahlung calculation assuming either an exponential or power law type electron energy spectrums. Since particle measurements are made simultaneously in two ends of the flux tube, lifetime calculations of substorm particles can also be made. These results are presented in Section 4.

Another example illustrating the close relationship between time variations of equatorial electron fluxes and precipitated fluxes is shown in Figure 2. This event and the event shown in Figure 4 consisted of easily

discernible rapid fluctuations in precipitated fluxes, including microbursts

(Anderson and Milton, 1964) and 5-15 second modulated fluxes (Brown et al.,

1965). The modulated structures have now been shown to occur also in

equatorial electron fluxes, and details concerning this analysis are

reported in Parks and Winckler (1969). The peak electron fluxes for the

April 21 event (Figure 2) were about 12×10^4 $(cm^2-sec-ster-keV)^{-1}$, and the

fluxes were superposed on the quiescent flux of about 4.5×10^4 $(cm^2-sec-ster-keV)^{-1}$.

The X-ray peak flux for the balloon depth of 2-3 gms/cm^2 was about

500 $(cm^2-sec)^{-1}$, superposed on the cosmic ray background flux of about

80 counts/second. It is also of worth to note that at about 1700 UT, the

balloon and the satellite conjugate were apart by about 1200 km. The

precipitation for this event was therefore at least this large in longitude.

Auroral precipitation was observed nearly continuously for a duration

of about 10 hours on August 11, 1967. The X-ray and the corresponding

electron flux variations in the equatorial plane are shown in Figure 3.

The two large precipitation events centered around 1945 UT and 0030 UT

(August 18) are again observed in time coincidence with increases of electron

fluxes of similar duration in the magnetosphere. As in previous events,

the time profiles between the two localities are well correlated. Here

one also notes modulated structures of a few minutes period (2130-2330 UT)

that are especially pronounced in the equatorial electron fluxes, and

the structures in the balloon data, although similar structures can be

identified, are not as well developed. (These modulated structures are

further studied and will be reported in another paper.) Another feature

to note here is that while peak fluxes in the equatorial electrons were

"typical" and about 10×10^4 and 6×10^4 $(cm^2-sec-ster-keV)^{-1}$ for the

two events, the precipitated fluxes were unusually intense. The peak

flux for the first event at the balloon depth of 2-3 gms/cm^2 for energies

h ν > 20 keV was about 5 x 10^3 $(cm^2-sec)^{-1}$, while the second event has a peak flux value of about half this value. These X-ray fluxes are about 10-20 times larger in intensity than for events observed in Figures 1 and 2. We also mention that fast temporal structures that commonly accompany precipitation events at these local times were not observed here. This is another example of "saturation" effects of modulated structures reported earlier (Parks et al., 1968a). A possible explanation for the unusually intense precipitation is given in Section 5.

The correlation of the August 17 event is shown in Figure 4. One notes here the usual feature showing that auroral precipitation was accompanied by increases of equatorial electron fluxes. The peak equatorial electron fluxes (at about 1640 UT) were about 7 x 10^4 $(cm^2-sec-ster-keV)^{-1}$ and this was superposed on the unstructured electron fluxes of about 1.5 x 10^4 $(cm^2-sec-ster-keV)^{-1}$. The balloon X-ray showed about 300 $(cm^2-sec)^{-1}$ at the peak.

Thus far the events shown have occurred in local time intervals between midnight and noon, and these generally showed excellent correlation between the equatorial plane and the auroral zone. This excellent correlation appears to break down at later local times. Figure 5 shows measurements taken between 1450 and 1830 local times for events detected on August 18, 1967. Here it can be seen that although precipitation in the auroral zone is accompanied by increases of outer zone electron fluxes, the detailed correlated features that were characteristic of earlier local times are no longer present. Moreover, as we proceed to later local times (past local dusk), the two time profiles no longer show any resemblance. Figure 6 shows the balloon X-ray and ATS-1 electron time profiles between 1900 and 2300 local times. Note also that the peak electron fluxes are considerably lower than those that occurred at earlier local times. The peak fluxes

were typically about 2×10^4 $(cm^2\text{-sec-ster-keV})^{-1}$ or less. It is notable that precipitated fluxes in these local times are usually diffused and unstructured over several minutes, and the intensity of precipitated fluxes is also usually very low (Parks et al., 1968a).

B. Discussion.

Several important features have been brought out with regard to the behavior of outer zone Van Allen fluxes and their relationship to auroral precipitated fluxes. These are: (1) auroral precipitation of energetic electrons is always accompanied by increases of trapped electron fluxes deep in the magnetosphere, and (2) the degree of correlation between the equatorial plane and the auroral zone is strongly dependent on the local time. The first observation agrees with results of an extensive study of auroral precipitation made by O'Brien (1964). He showed that increases in precipitated particles at 1000 km altitude were intimately associated with increases in mirroring fluxes at these altitudes (considered trapped particles). O'Brien interpreted this observation in terms of the "splash catcher" model for particle acceleration and precipitation. In this model, the magnetosphere is a sink for some accelerated particles (by a process yet to be identified), while precipitation represents accelerated particles in the loss cone. The results thus far presented in this article support this view. Whether O'Brien's model can be extended into the equatorial plane of the magnetosphere will·be examined in more detail later. O'Brien was not able to obtain direct information concerning the behavior of electron fluxes in the equatorial plane since his·measurements were confined to about 1000 km altitudes.

In view of the close relationship that exists between precipitation fluxes measured at ionospheric heights and increases of trapped fluxes observed deep in the magnetosphere, it is appropriate to ask at this time

where these particles were accelerated and what the precipitated fluxes represent. Some investigators (Mozer and Bruston, 1966; Evans, 1967) have recently speculated that the earth's ionosphere might be a source region for $\geq$ 40 keV auroral particles and there is even theoretical work (Perkins, 1968) showing that "loss cone" instabilities in the ionosphere under suitable conditions could lead to production of very high energy electrons. But then, why and how do these particles appear as predominantly 90° pitch (see Section 5) particles in the equator? Why is there a general agreement between the energy spectrums of precipitated and trapped electrons (McDiarmid and Budzinski, 1964)?

If, on the other hand, we assume that the equatorial region is where complicated wave-particle interactions occur to accelerate and precipitate particles (since it appears that most of the particles in a flux tube are affected by acceleration and precipitation during substorms), then one must ask whether the precipitated particles represent freshly accelerated particles in the loss cone or whether they are particles initially accelerated at large pitches which are scattered into the loss cone and precipitated. One feature that we are certain about is that the acceleration and precipitation processes must be strongly coupled since their time profiles are well correlated. The quantitative understanding of the acceleration and precipitation processes is beyond the scope of the present paper. However, in Section 6, after we have studied appropriately the behavior of particles at different energies (Section 4) and the pitch angle distributions of these particles in the equatorial plane (Section 5) during substorms, we will examine some possible mechanisms for particle acceleration and precipitation.

The second observation showing that the relationship between precipitated and trapped fluxes depends on local times is a different conclusion from

that derived earlier by O'Brien (1964). A re-examination of O'Brien's

Figures 22 and 23 will show that the local time dependence is present in

his data. In his Figures 22 and 23, there is a large "void" between local

times 1600 and 2200. Note that this is exactly the time interval where the

ATS-1 and the balloon observations are not well correlated. If one assumes

that equal statistical samplings were given to all local times in O'Brien's

study, this "void" represents either less frequent precipitation or lower

precipitation intensities. In any case, the present data do not support

O'Brien's conclusion that precipitation did not depend on local times.

C. Latitude Spatial Extend During Substorms.

It was mentioned in connection with Figures 1 and 2 that the pre-

cipitated measurements were taken when the balloon was more than 1200 km

west of ATS-1 conjugate in the auroral zone. The fact that the two time

profiles between trapped and precipitated fluxes correlate so well even

at these large distances is an indication that the acceleration was taking

place over a wide region of the magnetosphere, certainly at least 1200 km

in longitude at ground levels. This observation is consistent with the

earlier observations of O'Brien's (1964) where he also showed that the

precipitation region extended by more than five hours in longitude. The

observations of precipitation using balloon data indicated that the

precipitation is extended not only in longitude (Parks et al., 1968a)

but also in latitude (Winckler et al., 1962). We show in Figures 7 and 8

two substorm correlated increases observed by the ATS-1 that are

correlated with riometer absorption data taken simultaneously from about

L = 3.9 to L = 8.0 (courtesy of H. Sauer). The important feature to

note here is that the precipitation occurs over a wide range of L values.

From this observation it is tempting to conclude that increases may be

observable over equally extended regions of the magnetosphere, but this

conclusion cannot be verified using a single satellite. An extensive

study of precipitation events using the simultaneously measured riometer

chains indicates that precipitation can be small or large in L, a feature

already noted by O'Brien (1964). The riometer records indicate, however,

that generally the precipitation regions are large in L (Rosen et al., 1969).

The precipitation generally covers the trough region of the magnetosphere.

4. The Behavior of Higher Energy Electron Fluxes (150-500 keV

and 500-1000 keV) at Synchronous Altitudes, A Study of Electron Energy

Spectrums, and Calculation of Particle Lifetimes

The magnetosphere is distorted by the solar wind. The amount of

magnetospheric distortion is not fixed but changes according to changes

in the physical conditions within and outside the magnetosphere. Consequently,

the ATS-1 satellite, although geographically fixed, is not geomagnetically,

and in the course of a day, the circular satellite orbit will sample particles

from a range of L shells. During geomagnetic quiet days, the daily electron

time profiles exhibit a marked asymmetry about the noon-midnight meridian.

The effect arises presumably because there exists particle gradient in L,

and the diurnal variation is a measure of the distortion of the magnetosphere

in the geographic reference frame. The diurnal variations are also clearly

discernable in the locally measured magnetic field (Cummings et al., 1968).

It has been shown (Paulikas et al., 1968; Lanzerotti et al., 1967) that

these particle variations can be ordered fairly well by the local magnetic

field. The field and particle intensities increase and decrease together.

However, as the geomagnetic activity enhances, particle variations are

observed to occur totally independent of the local magnetic field. The

examples shown in Section 3 are of this kind.

It appears that there are two basic types of particle variations observed

in the magnetosphere at the ATS-1 orbit. In this article, we will

characterize the variations as spatial (or adiabatic) if the fluxes can be

ordered by the locally measured field; flux changes that occur independently

of the local field are characterized as temporal (or non-adiabatic). A

betatron type process is a physical mechanism that can produce adiabatic

changes in particles. Particle losses from whistler pitch-angle diffusion

are an example of pure temporal effect. One recognizes that the definition

of adiabatic and non-adiabatic changes of particle fluxes may not be the

standard definition. It is further recognized that the two effects can

be separated and each effect calculated if azimuthal and radial electron flux

distributions are known. However, with measurements taken from a single

point in space, we find the above definition useful and h   adopt

characterizing particle intensity changes. In the follow   different

such a criterion in describing the behavior of particle v

energies.

In this section it will be shown that (1) the large   served

at synchronous latitudes during substorms are predominant   -150 keV

energy range, and (2) the electron energy spectrums in th   plane

and the auroral zone are "similar". Since both trapped a   ied

particle fluxes are detected simultaneously, particle lif   lso

calculated. All data to be shown below are 1 minute coun   jes.

Each figure will consist of flux-time profiles from the 5   annel,

together with those from 150-500 keV channel and 500-100C   channel.

When the rate in the 500-1000 keV channel is below 0.1 cc   they

are usually omitted from the graph. To characterize whet   ations

are spatial or temporal, the behavior of local magnetic field intensities

are consulted. Figure 9 shows the behavior of locally measured H component

magnetic field values (courtesy of Coleman and Cummings, UCLA) for all of the periods to be discussed. The numbers in brackets on the left side of each curve correspond to the mangitude of the field value at the start of the interval considered. The interval of time considered as well as the date are given on the right of each curve. For example, the top curve shows that on April 19, 1967, the magnitude of H component at 1400 UT was ≈74γ, which slowly increased as the ATS-1 rotated into later times, reaching a value of ≈83γ at 1600 UT.

A. Electron Energy Dependence During Substorms at the Equator.

In Figures 10 and 11 are shown the events discussed earlier in Figure 1. An obvious feature of these graphs is that the major increase of electron fluxes observed in the equatorial plane during this substorm was in the 50-150 keV energy range and the increases in this channel are non-adiabatic. (Our observation does not mean, however, that larger fluxes are not observable, for example, at energies < 50 keV.) The fluxes in the 50-150 keV channel increased by a factor of 2-4 while no such increases are registered in the 150-500 keV energy channel (or 500-1000 keV channel). The slow increase observed between 1430 and 1540 UT (Figure 10) in the 150-500 keV channel is due to the distortion of the magnetosphere. Figure 9 shows that during this interval, the local H-component magnetic field intensity increased from 74γ at 1400 UT to about 83γ at 1600 UT. Consequently, the circular orbit of the ATS-1 satellite was sampling particles from different L shells and the slow increase of electron fluxes in the 150-500 keV energies arises because there is a radial gradient in electron flux distribution. For the event centered around 2018 UT (Figure 11), the steady and unchanging electron fluxes were observed in the 150-500 keV energies because the magnetic field values during this interval of time were constant, as shown in Figure 9. This means that during

this portion of the ATS-1 orbit, the satellite stayed on nearly constant

L shell. Here also, the appearance of large increases of electrons in

the 50-150 keV energies is temporal and non-adiabatic.

The behavior of the April 21, 1967 event for electron energies from

50-1000 keV is shown in Figure 12. The predominant increase of electron

fluxes is again observed in the 50-150 keV channel. Note, however, that

a small increase is also observed in the 150-500 keV energy channel.

It is also apparent that the behavior of electrons in this energy range is

quite different from the behavior of those in the 50-150 keV energy channel.

The difference is shown not only in the relative increase of electron fluxes

attained but also in their flux-time profiles. The peak electron flux in

the 50-150 keV range is about 5 times that of the ambient flux level while

the peak level in the 150-500 keV energy range is only about a factor of

1.5 the initial ambient flux level. Also the peak in the 150-500 keV

energy channel occurs after 7 minutes from the "onset", while the fluxes

in the 50-150 keV channel are still increasing. From Figure 9 we see the

150-500 keV flux increases are not from trapped particle radial distribution

discussed above. The adiabatic effect due to the sampling of different

L shells is still present but more clearly discernable in the 500-1000 keV

channel.

In Figure 13 are shown the time profiles of the different energy channels

for the event detected on August 11, 1967 (1900-2030 UT), while the satellite

was in the late local morning hours. The largest increase is in the

50-150 keV energy channel. It is further evident that a small increase

is observed in the 150-500 keV energy channel, exhibiting much the same

pattern as in the April 21 event shown in the previous figure. During this

part of the orbit the local magnetic field intensity varied only by about

7γ. However, the fact that no adiabatic effects were observed means

that for the small interval of L shells sampled, the particle fluxes had

a nearly constant radial distribution. Note that even the fluxes in the 500-1000 keV energy channel were nearly constant.

Figure 14 shows another example of a substorm-correlated increase of electron fluxes that was predominantly observed in the 50-150 keV energy channel. This behavior resembles that of events already shown. One notes the usual factor of 4-5 increase of electron fluxes in 50-150 keV energies while only a small increase is observed in the higher energies. The slowly increasing flux in the 150-500 keV energy channel is the usual adiabatic change due to the distortion of the magnetospheric cavity, as evidenced in the magnetic field measurements (Figure 9). The abrupt "hardening" of energy spectrum at about 1625 UT is apparently real since similar hardening of the spectrum was observed in precipitated fluxes (not shown).

Substorm-correlated particle events that occur in the late afternoon and evening sectors exhibit a feature commonly absent in substorm increases that occur between local midnight and noon. Figures 15 and 16 show the time profiles of the three energy channels for electron increases detected in the afternoon and late afternoon sectors. The examination of Figure 15 will show that although, as in previous cases, the fluxes increased predominantly in the 50-150 keV energy channel, there was an initial decrease of electron fluxes at about 2331 UT that occurred simultaneously in all three energy channels. The increasing count-rate began about 2337 UT (again in all three energy channels) and evidently indicated the onset of a substorm, as can be seen from the abundant increases of electron fluxes in the energy interval 50-150 keV following the recovery. Similar "signatures" in all three energy channels are also observed at about 2352 UT and at 0012 UT (August 12, 1967). These signatures are superposed on essentially constant electron fluxes in the 150 to 500 keV and

500 keV to .1 MeV time profiles, while they are superposed on the varying fluxes in the energy channel 50-150 keV. In this regard, the characteristics of this substorm event are no different from the characteristics of the events discussed earlier, except for these signatures. Examination of Figure 9 shows that these particle signatures are particle redistribution effects associated with L-shell modulations (motion of L-shell due to $\vec{v} \times \vec{B}$ electric field) and are adiabatic effects since similar "signatures" are observed in the magnetic variations.

Figure 16 shows another example of L-shell modulation of particle fluxes preceding substorm electron increases in the 50-150 keV energies. The variations in the 150-500 keV and 500-1000 keV energy channels appear completely as adiabatic effects. Their time profiles are correlated with the time variation of the local magnetic field, as shown in Figure 9. The decrease of electron fluxes at about 0640 UT registered simultaneously in the 50-150 keV and 150-500 keV energy channels are also adiabatic effects. Note, however, that the variations in the 50-150 keV energies have both the adiabatic and non-adiabatic effects. The increases after about 0720 UT in this channel are mostly non-adiabatic.

The last two figures show that certain electron features in the afternoon sector are considerably different from energetic particles associated with substorms in the morning sector. First to note is the considerable amount of distortion of the magnetosphere in the evening sector accompanying a substorm. Although it is not known what the causal relationship is between occurrence of substorms and the distortion of the magnetosphere, the distortion of the magnetosphere has its largest effect in the local evening sector (Cummings et al., 1968). This distortion is probably associated with the addition and loss of ring current protons which populate the evening sector. Finally, the evening substorm-correlated

energetic electron fluxes are considerably smaller in their intensities than the events detected in the local morning sectors.

It should be apparent from above examples that the major increase of electron fluxes observed in the outer radiation zone during substorms is in the 50-150 keV energies. Since these increases are primarily caused by non-adiabatic process, we interpret that these are freshly accelerated energetic particles. The above results on the behavior of particle energies during precipitation have also been reported by O'Brien (1964). He noted that the predominant effect during precipitation was observed for electrons of energies $\simeq$40 keV. O'Brien also pointed out that higher energy electrons were essentially unaffected, and they behaved completely differently from the $\simeq$40 keV electrons, a result which is in accord with observations between 50-150 keV and 150-500 keV electrons in the equatorial plane. Possible reasons for the differing behavior in energies are given in Section 6.

B. Derivation of Precipitation Electron Energy Spectrum.

The thick target bremsstrahlung theory provides a means for obtaining the primary precipitation electron energy spectrum from observed balloon X-rays. In this calculation, estimates of both fluxes and probable energies of electrons responsible for the bremsstrahlung X-rays can be obtained. The differential energy spectrum of electron flux $N(E)$ and that of the photon flux $n(h\nu)$ are related by the integral equation $n(h\nu) = \int_{h\nu} K(h\nu,E)N(E) \, dE$ where $K(h\nu,E)$ involves the cross-section (Bethe and Ashkin, 1953), and is fairly well known. The solution of this integral equation yields the electron energy spectrum.

The X-ray spectrum is measured experimentally. However, for our purpose we will initially assume that the electron spectrum has an exponential form, e^{-E/E_0}. Then, using Kramer's estimate of $K(h\nu,E)$ as given in

Evans (1955), $K(h\nu,E) = 1.4 \times 10^{-6} Z(E - h\nu)/h\nu$, the bremsstrahlung

X-ray spectrum near the production layer is obtained:

$$n(h\nu) \simeq \frac{E_O^2 \, e^{-h\nu/E_O}}{h\nu/E_O} \qquad (1)$$

At the balloon depth, the measured X-ray intensity is

$$N(>h\nu) \simeq \int_{h\nu} n(h\nu) \, e^{-\mu x} \, F(h\nu) \, G(\theta) \, d(h\nu) \qquad (2)$$

where atmospheric attenuation factor, $e^{-\mu x}$, the detector resolution, $F(h\nu)$,

and the geometry factor $G(\theta)$ have been incorporated. The limits of

integration are defined by the instrument energy settings. All quantities

in equation (2) are known except for E_O.

The balloon X-ray detector consisted of X-ray measurements for quantum

energies >20 keV and >50 keV. The X-ray count-rate ratio $N(20-50 \text{ keV})/N(>50 \text{ keV})$

is a measure of spectral hardness at the balloon depth. Such ratios can

be constructed and compared to the theoretical ratios obtained from equation (2)

for various electron e-folding energies, E_O. Consequently, E_O values

responsible for observed X-ray ratios are obtained. The values obtained

in this manner are accurate to about 30% provided that the Compton scattering

is minimized. Our balloon floating altitudes were about 2-3 gms/cm^2.

For 20-150 keV X-rays, the mean Compton scattering length is about 6 gms/cm^2

of air. The calculation also assumed the precipitation electron fluxes to

be uniformly distributed at electron stopping heights ($\simeq 100$ km altitude).

Typical X-ray count-rate ratios for the events studied varied between

2 and 4, corresponding to primary precipitation electron exponential energy

spectrum with e-folding energies between 15-20 keV. Consequently, the

most probable electron energies responsible for the observed X-rays

($h\nu > 20$ keV) are about 40-50 keV. One notes that the 20 keV electron

e-folding energies are typical of auroral precipitation spectrums

(Barcus and Rosenberg, 1966; Parks et al., 1968a; Hudson et al., 1965; Anderson and Enmark, 1962) for these local times (≈0600 L.T.). Direct measurement of precipitation electrons on rockets also shows ≈20 keV e-folding energies (Lampton, 1967).

The electron e-folding energies for the corresponding events observed for trapped fluxes by the ATS-1 varied between 20-25 keV. (The equatorial analyses represent upper limit values since they were obtained from the ratios of fluxes in 50-150 keV and 150-500 keV channels. Recall that ≈90% of the fluxes are observed in the 50-150 keV energies.) Our analysis indicates that the precipitation and trapped electron energy spectrums are similar (within the limits of observational differences and errors in the bremsstrahlung calculations), and agrees with previous conclusions of McDiarmid and Budzinski (1964).

C. Lifetime Calculation.

The estimates of precipitated electron fluxes responsible for observed X-ray intensities are also available from the bremsstrahlung calculation. Since we made simultaneous observations of precipitation and trapped fluxes, lifetimes for substorm electrons can be computed using methods outlined in Hess (1968) and O'Brien (1962). Table 1 summarizes the results of such calculations where we have also included the average fluxes observed at the equatorial plane and the auroral zone. The lifetimes of these electrons varied from about 200 seconds to about 2000 seconds. Typically, the lifetimes during substorms are about 10^3 seconds.

These lifetimes should be compared to electron drift periods. For 70 keV electrons (which is about the average energy of electrons in the 50-150 keV channel if one assumes a 20 keV e-folding energy) the drift period in a dipole field at 6.6 R_e equator in the absence of an electric field) is about 6×10^3 seconds. Consequently, it follows from the results in Table 1 that electrons observed during substorms are locally accelerated

particles and that the ATS-1 satellite is measuring freshly accelerated particles created in the near vicinity of the satellite. The short lifetimes of these substorm electrons also argue against the tail region as being the primary region for acceleration. Instead, the short lifetimes are consistent with a magnetospheric acceleration process that is a large-scale disturbance, covering many hours in longitude. The early observation of electron precipitation of O'Brien (1964) and the more recent of McDiarmid et al., (1969) are in agreement with this conclusion.

5. Behavior of Pitch-Angle Distribution and Anisotropy
of the 6.6 R_e Equatorial Electrons During Magnetospheric Substorms

The purpose of this section is to examine the pitch-angle distribution of the equatorial electrons during the substorm increases. Their dependence upon electron energy and time (therefore the flux) is also studied.

The combination of a spin-stabilized geostationary satellite and a detector with a narrow aperture permits measurement of electron pitch-angles when the local magnetic field direction is known. The magnetic field on the ATS is measured by the UCLA group. As mentioned in Lezniak et al., (1968) the full view angle of the University of Minnesota electron spectrometer is about 11° and its axis points 16° south of the equatorial plane and sweeps out a cone about the axis of the spacecraft. Since the earth's magnetic field is rarely parallel to the spin axis of the satellite (or normal to the equatorial plane), particles of differing pitch angles are sampled during a revolution. The spin period of the satellite is about 0.62 seconds and can be accurately measured by an onboard sun sensor. The sampling period of the spectrometer system for a given energy channel is 160 milliseconds. Thus, in one revolution, the spectrometer samples about four times at four differing pitch-angles. Depending on the vector direction of the earth's magnetic field, a large range of pitches can be

sampled. Nominally, particle pitches between 60 and 90° are sampled.

Figure 17 shows a schematic diagram of the detector orientation on the

ATS-1 satellite where α_{max} and α_{min} are respectively maximum and minimum

pitch angle sampled for an arbitrary earth's magnetic field direction.

A. Pitch-Angle Distributions During Substorms.

Examples of pitch-angle distributions observed during substorms

in the equatorial plane of the magnetosphere are shown in Figures 18

through 23. In each figure are shown several distributions constructed

at different times in order to illustrate their behavior upon the various

phases of the substorms. These figures represent distributions of substorm

events that occurred over local times from about 0400 to about 1400.

The data shown are for pitch-angles averaged over 6° interval and fluxes

averaged over 72 seconds. Fifteen-second averages of the field components

measured by the UCLA group were used for the pitch-angle construction.

The pitch-angle distributions shown in Figure 18 are for the substorm

event of April 19, 1967 and the distributions are for electrons 50-150 keV

taken before the substorm (1427 UT), during the rising portion (1442),

during the first maximum (1514 UT), and during the declining portion of the

second maximum (1520 UT). The distributions at several time intervals

for electrons in the 150-500 keV energy range are shown in Figure 19.

Here the distributions are for ambient electron fluxes since no significant

increases of electron fluxes were observed during the substorm. Examination

of these two figures and subsequent figures will indicate a certain

characteristic behavior of the pitch-angle distributions during substorms

These are: (1) More electron fluxes are observed at 90° pitch angles

than at smaller pitches, indicating that the distributions are anisotropic.

(2) The maximum at 90° is observed at all phases of the substorm.

(3) The degree of anisotropy (defined later) changes with time and is therefore

dependent upon the electron flux. And (4) the electron pitch-angle distributions are anisotropic for both 50-150 keV and 150-500 keV energy electrons. The degrees of anisotropy in these two energy ranges may be different, however, indicating that there is possibly energy dependence.

The pitch-angle distributions at several time intervals for the later substorm event (also observed on April 19, 1967) are shown in Figure 20. Here, although a narrower range of pitch-angles was sampled, the characteristics exhibited are essentially similar to those already shown in the earlier two figures. Note, however, that a small difference does exist in their behavior. The distributions shown in Figure 20 appear to fall off more rapidly with decreasing pitch-angle than those shown in Figures 18 and 19. For 50-150 keV electrons, the distribution was nearly flat between 74° and 90° for the event shown in Figure 18. On the other hand, Figure 20 shows that the electron fluxes differed by more than 8% for the pitch-angle ranges 74-90° and 80-86°. This difference may be a local time effect since the two substorms occurred in local time separated by more than five hours. The distributions for the 150-500 keV energies are again for the ambient Van Allen fluxes. ·

The distributions shown in Figures 21 and 22 are for the April 21, 1967 substorm event for the two electron energy channels. For the 50-150 keV electrons, it suffices to note that the characteristics shown are as described in previous substorms. In Section 4, we showed that during this substorm, increases of electron fluxes were observed in 150-500 keV energies. The distributions shown in Figure 22 represent the pitch-angle distributions for these substorm energetic electrons. It is worthy of note that the behavior of pitch-angle distributions for these higher energy electrons is not too different from 50-150 keV electrons: the pitch-angle distribution for these energies is also anisotropic with peak fluxes toward 90° pitches.

It was already mentioned in Section 3 that unusually large precipitated fluxes were observed on August 11, 1967 while the increase in the equatorial plane was "typical". Figure 23 shows the pitch-angle distributions for the substorm that was centered around 1936 UT. These distributions, although they possess all the qualities of the distributions thus far studied, appear less anisotropic than those previously shown. In fact, it can be seen that the distributions in the 50-150 keV energy channel became less anisotropic (more isotropic) with increasing fluxes. (This will be shown in more detail later.) Consequently, the unusually intense auroral precipitation can in part be accounted for by this observation. The pitch-angle distributions for the 150-500 keV electrons are for substorm correlated-electron increases since a noticeable increase of electron fluxes was observed in this energy range during this substorm. Note, however, that the behavior of the distributions in this energy channel is different from the 50-150 keV electrons. The distributions maintained their high anisotropy even during the peak fluxes observed in this energy range.

The substorm event centered around 0030 UT on August 12, 1967 (Figure 15) was initially preceded by the modulation of L shell which produced flux variations simultaneously in all energy channels. The effect of such L shell modulation in particle pitch-angle distributions is shown in Figure 24 for the first two electron energy channels. First, we describe the behavior of the distribution for the 50-150 keV electrons. At 2332 UT, the distribution was peaked toward 90° pitch-angle. The first indication that the magnetosphere was becoming distorted was, according to Figure 9, around 2334 UT. At this time, the pitch-angle distribution was still anisotropic and peaked toward 90° pitches, as shown in Figure 24. By 2336 UT, it is clear from Figure 9, that the magneto-sphere was quite distorted, and at this time, the pitch-angle distribution

became nearly isotropic. Thereafter, the magnetic field recovered to its pre-distorted value and also accompanying this recovery, we see a continual increase of electron fluxes in the 50-150 keV energy channel (Figure 15). The pitch-angle distributions taken at 2349 and 2356 UT represent the behavior during the rising portions of the flux-time curve. Here we note that the distributions were anisotropic again and peaked toward 90°, showing the typical characteristics of substorm events studied earlier.

The effects of the L shell modulation upon the pitch-angle distribution for the 150-500 keV electrons are shown in the right half of Figure 24. At 2332 UT (before the inflation of the magnetosphere), the distribution in this energy channel was anisotropic and peaked toward 90° pitches. At 2334 UT (the first sign of magnetospheric cavity distortion) we see the distribution peaked at intermediate pitch-angles, which finally becomes peaked toward smaller pitches at 2335 UT. At 2336 UT, the anisotropy toward smaller pitch angles is at maximum, and this anisotropy gradually decreases during the recovery of the magnetosphere cavity distortion (2339 UT). When fully recovered at 2356 UT, the pitch-angle distribution is again peaked toward 90°.

B. Pitch-Angle Anisotropy as a Function of Time.

A quantitative measure of the pitch-angle anisotropy and its behavior in time are shown in Figures 25-29 for the various substorm events discussed earlier. These figures contain, in addition to the one-minute averages of the count-rate time profiles, the anisotropies measured in percent as a function of time. The definition of the pitch-angle anisotropy will be different for different substorms since the definition depends on the range of pitch-angles sampled. In each case, the anisotropy is defined as $A = 1 - J(\Delta\alpha_{min})/J(\Delta\alpha_{max})$, where $\Delta\alpha_{min}$ and $\Delta\alpha_{max}$ correspond to minimum and maximum 6° range of pitch-angles sampled.

The behavior of the anisotropy shown in Figure 25 is for substorm events observed in 50-150 keV electrons on April 19, 1967. This figure shows that in the gross sense, the anisotropy-time profiles resemble the electron-flux-time profiles. For example, the anisotropy-time profile for the earlier substorm event (left curve) has two maxima as does the flux-time profile. A more detailed examination, however, shows that there are considerable differences between flux and anisotropy-time profiles. We note, for example, that A was about 30% at 1420 UT, and decreased to about 22% by 1428 UT. This change occurred while particle fluxes and the local magnetic field (see Figure 9) were essentially constant. Moreover, the peak anisotropies did not coincide with peak electron fluxes. For both of these events shown, the peaks in anisotropies lagged the peaks in the flux-time profiles by a few minutes. The abrupt decrease of A between 2040 and 2045 UT is associated with the decrease of electron fluxes during this time (notice the dip in the flux-time curve). This is purely a pitch-angle modulation effect. Finally, note that the peak anisotropies for the early substorm events were around 30%, while the maximum for the second substorm (right curve) was about 28%. (Note, however, that the two anisotropies for these two time periods are defined differently.)

Figures 26 and 27 show electron flux and anisotropy-time profiles of the April 21, 1967 substorm event for the two electron energy ranges. Prior to any indication of electron increase at, for example 1606 UT, A ≃ 28% for 50-150 keV electrons (Figure 26). A remained at this value until about 1617 UT, during which time the electron fluxes increased by more than a factor of 3. Beginning about 1617 UT, A began to increase slowly, reaching ≃ 40% at 1628 UT. The anisotropy then dropped to about 35% at 1628 UT, and thereafter, A slowly increased, finally reaching 40% at about 1655 UT. Between 1655 UT and the termination of the substorm

event (at approximately 1710 UT), A decreased and reached a pre-substorm
value of about 30% (not shown). One notes that the peak anisotropy for
this event is greater than those of April 19, 1967. This difference
is probably due to the difference in the peak electron fluxes attained
during substorms. The peak fluxes in 50-150 keV energies for April 19
were $\approx 7 \times 10^6$ $(cm^2-sec-ster)^{-1}$, while on April 21, the peak flux was
$\approx 14 \times 10^6$ $(cm^2-sec-ster)^{-1}$. For 150-500 keV electrons, Figure 27 shows
that the anisotropy-time curve resembled the flux-time profile. At 1605 UT,
A was $\approx 30\%$, which slowly increased as more fluxes were observed in this
channel, reaching a maximum of about 43% at 1613 UT, coinciding roughly with
the time of maximum electron fluxes observed in this energy channel.
Then A began to decrease as did the fluxes and at 1630 UT, A was $\approx 31\%$;
this was essentially the value of A before any electron flux increases were
observed in this channel.

The behavior of pitch-angle anisotropy for the two electron energy
ranges is shown in Figure 28 for the August 11, 1967 substorm, during which
an unusually intense auroral precipitation was accompanied. For the 50-150 keV
electrons, A was averaging around 22% between 1900 and 1927 UT. When
the counts/sample increased to about 35 corresponding to a flux of
about 1.6×10^5 $(cm^2-sec-ster-keV)^{-1}$ at 1624 UT, a sharp decrease in A
began. A minimum value of about 10% was reached at about 1930 UT. The
anisotropy remained essentially at 10% for about 25 minutes, past the time
when maximum electron fluxes were observed and even including a large
interval during the decaying portion of the flux-time curve. (Note that
after about 1940 UT, A had to be redefined. From about 1940 to 2000 UT,
$A = 1 - J(66-72°) / J(78-84°)$, and they are represented as triangles,
instead of circles.) The anisotropy began to increase beginning around

1952 UT, and by 2002 UT, A was ≃20%. (Magnetic field information after 2002 was not available. Consequently, there is no pitch-angle information after this time.)

The behavior of pitch-angle anisotropy for the time interval during which electron increases were observed in 150-500 keV electrons on August 11, 1967 is shown in Figure 28 (right curve). One notes here that the behavior is quite opposite from the behavior observed for 50-150 keV electrons. Instead of the decrease, we see A increasing as more fluxes are observed in this energy channel. The behavior for this event is essentially similar to what was observed on April 21, 1967 for electrons in 150-500 keV energy channel. In both of these events, A increased and decreased with increasing and decreasing electron fluxes in their respective energy ranges. The independent behavior of the pitch-angle distribution shown in Figure 28 for 50-150 and 150-500 keV electron energies is another indication that the magnetospheric accelerating phenomena is an energy dependent process which operates in differing manner at different energies. Previously, we showed that the time profiles in these energy channels were different (Section 4).

The final event for which we wish to illustrate the complex behavior of pitch-angle anisotropy as a function of time is the substorm event detected on August 11, 1967 that occurred around 1400 local time and one that was preceded by the modulation of the L-shell (Figure 15). As mentioned before, the first indication of magnetospheric distortion occurred around 2334 UT at which time the electron fluxes were observed to decrease simultaneously in all energy channels (Figure 15). The degree of change in the observed anisotropy during these times is indicated in Figure 29 (left curve) for 50-150 keV electrons. As the electron flux in this energy channel decreased, the pitch-angle anisotropy also decreased. At the crest, the anisotropy factor was less than 0%, indicating that the pitch-angle distribution

was actually peaked toward smaller pitches. When the flux began to return to its initial value accompanying the recovery of the magnetospheric distortion, the anisotropy increased and the pitch-angle distribution was again peaked toward 90° pitches. The anisotropy began to increase as more accelerated particles were observed, but note that at 2352 UT the pitch-angle anisotropy was again interrupted. This decrease is associated with the dip in the flux-time profile, which in turn is associated with the decrease of the magnetic field value (Figure 9). After this second dip in the anisotropy, it began to increase again as did the particle fluxes. (Locally measured magnetic field values were not available after 2400 UT. Information of anisotropy after this time is not available.)

The effect of 150-500 keV electron pitch-angle anisotropy is considerably more severe when the magnetosphere shape is altered as shown in Figure 29 (right curve). The anisotropy started at 27% initially, which, at the crest was about -14%. The negative anisotropy means pitch-angle distribution was peaked toward smaller pitches. At the second crest (2352 UT), the anisotropy again dipped but the pitch-angle distribution was still peaked toward 90°.

As mentioned earlier, the collapse and recovery of the magnetosphere is believed associated with ring-current proton population in the magnetosphere as Cummings et al. (1968) have suggested. In view of the fact that the ring current population was altered prior to large increases of electron fluxes (50-150 keV), the magnetospheric acceleration process may be associated with plasma instabilities triggered by the proton redistribution effects in the ring. One notes that if the decrease of the local magnetic field is attributed to diamagnetic effects, the decrease corresponds to addition of protons to the ring. The recovery to

the normal field intensity is then the loss of these protons. It is precisely following the recovery that large increases of electron fluxes in the 50-150 keV are observed (see Figure 15). Finally we note that the decrease in magnetic field $|\vec{H}|$ (and the particles) correspond to the appearance of an eastward directed electric field. Consequently, it appears that electric fields play a role in substorms, as was noted in a recently published article by Mozer and Serlin (1969). It is worthy of note that Mozer and Serlin also indicated a large eastward directed electric field in the dusk sector during substorms.

While the behavior of pitch-angle distributions and the anisotropies from event to event differ in detail, the above examples and those of April 2, August 17, 1967 substorms (not shown) show that (1) the electron pitch-angle distribution during substorms in the equatorial plane of the magnetosphere is peaked toward 90° pitches, and (2) that, except for the August 11 event in 50-150 keV energies, the pitch angle anisotropy in general increases with increasing electron fluxes during substorms. From examination of a limited number of substorm events, it appears that these characteristics hold true for both 50-150 keV and 150-500 keV electrons. These observations included local time sectors covering a large region of the magnetosphere, from midnight to past the local noon. Some of the differing behaviors from one event to the next may be attributed to local time effects, but they appear minor at least in the local time sectors examined. From one example of substorm event observed in the evening sector (Figure 16), the pitch-angle distribution in this local time region was isotropic, and remained isotropic throughout the entire substorm duration (not shown). We are currently examining in more detail the behavior of the pitch-angle distribution in this local time sector and the results will be reported in another paper.

6. Summary and Discussion.

1. The simultaneous observation between the equatorial plane of the magnetosphere and the auroral zone has shown that auroral energetic electron precipitation is always accompanied by an increase of energetic electron fluxes in the magnetosphere. The time-flux profiles between trapped magnetospheric electrons and precipitated auroral energetic electrons are extremely well correlated in the local time sector ≈0000-1400 hours. Between 1400 local times and midnight, the precipitation and trapped fluxes are a factor of 3-4 smaller than those in the morning sector, and their correlation in this local time sector is poor.

2. The precipitation region as observed by a chain of riometers from L = 3.9 to L = 8 covers generally the trough region of the magnetosphere. Consequently, auroral energetic precipitation covers a large L-shell region.

3. The magnetospheric acceleration process is energy dependent in that major increases of electron fluxes are observed in the 50-150 keV energies (as far as the University of Minnesota detector system is concerned). Electron fluxes when observed in the 150-500 keV energy channel are a factor of 80-100 smaller than those in the 50-150 keV channel. The electron flux-time profiles in these two energy channels are quite different.

4. Within the limits of experimental uncertainties and the thick target bremsstrahlung calculations, our results show that the electron energy spectrums between the equatorial plane and the auroral zone are similar. Assuming an exponential form of electron energy spectrums, the e-folding energies are about 20 keV.

5. The lifetimes of these energetic electrons during substorms ranged from about 200 seconds to about 2000 seconds. Since these observations correspond to measurements conducted over widely separated local time regions (from about midnight to past local noon), and since these lifetimes are much shorter than 50 keV gradient drift times, one concludes that the spatial region of acceleration extends equally large distance in longitude. Consequently, the magnetospheric acceleration is a large-scale disturbance in both longitude and latitude.

6. The pitch-angle distributions during substorms (at all phases) are anisotropic and flat with peak toward 90°. The pitch-angle anisotropy increases with increasing electron fluxes during substorms. This behavior describes both the 50-150 keV and 150-500 keV electrons in the magnetosphere with the exception of one event (August 11, 1967).

7. The pitch-angle distribution of one event examined in the dusk sector showed it to be isotropic at all phases of the substorm. The substorm in this local time sector is usually preceded by an L-shell distortion, which may be associated with redistribution of proton population in the ring.

A. Acceleration and Precipitation Mechanisms.

For local times considered ($\approx$0000-1400) the pitch-angle distributions are flat (peaked at 90°) at all phases of the substorm. If we assume the distributions to have the form $\sin^n \alpha$, the distributions in the equatorial plane have the exponent n varying between 2 and 3. The significance of this is not understood at present. Since the distribution during substorms is flat, one of the requirements of the magnetospheric acceleration mechanism is that it be capable of producing a flat pitch-angle distribution. At present, there is no complete theory of particle acceleration in the magnetosphere or the auroral zone. The few theories published (see review articles by Kennel (1969), and Axford (1969)), that can account in part for the observations presented in this paper are discussed briefly below.

The convective flow (Axford and Hines, 1961) energizes particles by having the flow electric field $\vec{E} \times \vec{B}$ drift the particles into an increasing magnetic field region. Since deep in the magnetosphere tail region where B $\simeq$ constant, a particle would gain mostly parallel energy by conserving its second adiabatic invariant. As the particles are brought in closer to the earth and especially in to the auroral region where $\vec{\nabla B}$ is large, the conservation of the first invariant implies that the perpendicular energy is increased. The resulting auroral zone particle pitch-angle distribution will be flat and peaked toward 90°. One must note, however, the most energy a particle can gain is $\simeq 50$ keV, corresponding to the potential of the flow. This process cannot adequately account for the relatively abundant particles of energies > 50 keV and > 150 keV during substorms.

The diffusion of particles across L shells by conserving first and second adiabatic invariants can effectively accelerate or decelerate particles. If the diffusion of particles is into higher $|\vec{B}|$ regions, the particles gain perpendicular energy and the resulting pitch-angle distribution will be peaked toward 90° pitches. Particle diffusion across L shells invoking presence of transverse electric fields has been theoretically considered (Swift, 1965 and Falthammar, 1965). Although this process produces a flat pitch-angle distribution, it is unlikely that it is the principal acceleration mechanism responsible for > 50 keV energy particles. The diffusion times are considerably longer than substorm durations. On the other hand, if cross-L diffusion takes place at Bohm rate (Cornwall, 1968), many of the auroral and magnetospheric observations can be explained. The Bohm diffusion coefficient is roughly $D_B \simeq \Omega_- R_-^2$ where Ω_- and R_- are electron gyrofrequency and radius, respectively (see Kennel, 1969).

Particles can be accelerated during strong pitch-angle diffusion
(Kennel, 1969). If low-energy magnetospheric electrons (1-10 keV) produce
a large-amplitude whistler spectrum, then the electrons interacting with
these intense whistlers undergo both pitch-angle and energy diffusion.
Energy diffusion occurs because particles can absorb whistlers and gain
energy. In cyclotron resonance interactions, the particles can gain
perpendicular energy by losing parallel energy. The amount of energy gained
is dependent only on the whistler wave spectrum present. In any case, a
pancake pitch-angle distribution is produced.

It seems possible that the strong pitch-angle diffusion is operative
in the magnetosphere and that the cyclotron-resonant interactions can
adequately accelerate and precipitate particles (Kennel, 1969). Further
support comes from the recent OGO-3 and OGO-5 observations of large ampli-
tude whistler noise and chorus spectrum confined near the equatorial plane
(Russel et al., 1969; Brody et al., 1969). Fortuitously, these whistlers
were observed when intense auroral precipitation was detected by balloon-
borne detectors that this investigator was flying from the auroral zone.
(These overlapping data are being examined in detail.) Additional evidence
that the whistler interaction may be operative during precipitation is provided
by the correlation between enhancement of VLF chorus emission during precipi-
tation (Oliven and Gurnett, 1968).

Although the whistler theory is quite incomplete at the present state
since time dependence and coupling of pitch-angle and energy diffusion has
not been completely worked out, the theory still has merit since it can ex-
plain a considerable part of the results presented in this article. Qualita-
tively, the whistler theory can explain, for example, the similarities in

precipitation and trapped electron flux-time profiles and the differing

behavior of the ≃50 keV and ≃150 keV electrons. We examine below some of

the consequences of the whistler theory concerning acceleration and precipi-

tation and compare these with observations.

To begin with, one notes that the ambient electron flux level of the

≃50 keV electrons at the ATS-1 orbit is usually around the stably limited

flux values of about 3×10^7 $(cm^2\text{-sec})^{-1}$ predicted by the whistler thoery

(Kennel and Petschek, 1966). Consequently, when the acceleration source

creates new particles, the electron flux will exceed the stably trapped

flux level and plasma waves will be generated. Since the acceleration

preferentially creates particles with 90° pitches, particles will be scattered

into the loss cone by the resonance interaction. The whistler theory predicts

that precipitation rate is proportional to the diffusion rate, and that the

diffusion coefficient is proportional to the whistler wave spectrum. Since

the growth rate is proportional to the pitch-angle anisotropy, the whistler

wave amplitude will increase as the anisotropy does and leads to enhancement

in the precipitation rate. An acceleration process that preferentially

produces a flat pitch-angle distribution automatically increases the whistler

growth rate and therefore the precipitated fluxes.

The lifetime calculations shown in Table 1 indicate that the ATS-1

electrons are in between weak and strong diffusion, with the exception of

the August 11 events when the electrons appear to be in strong diffusion.

The 200 second lifetime shown in Table 1 agrees quite well with the theoreti-

cal calculations of electron lifetimes in strong diffusion (Kennel, 1969).

Note, however, that the observed anisotropy factor was not zero (A ≠ 0), as

was predicted by Kennel (1969). Kennel's calculation was for the case

when the diffusion coefficient was infinite ($D \simeq \infty$) and when the approxima-
tions $\omega/\Omega \ll 1$ and ${}^{E}c/_{E} \ll 1$ hold (Kennel, private communication). Since
these conditions may not be fully met at the ATS-1 orbit and since the pitch-
angle diffusion rate is certainly less than infinite ($D < \infty$), it is not
surprising that some pitch-angle anisotropy is still maintained outside the
loss cone even during strong pitch-angle diffusion (see Figure 28).

Let us consider here the time dependent situation where it is assumed
(for simplicity) that the electrons are near strong diffusion. Let us
also define an anisotropy factor as $A = 1 - J(\alpha < 90°)/J(\alpha = 90°)$, where
α is less than 90°. It should be evident that the $\alpha < 90°$ particles diffuse
more rapidly toward the loss cone than the $\alpha = 90°$ particles, since the
lifetimes of $\alpha < 90°$ particles are considerably shorter than the $\alpha = 90°$
particles. The reason for this is that the resonance condition in whistlers
$\omega - k_{11} v_{11} - |\Omega_-| = 0$ implies that $\omega \simeq |\Omega_-|$ for $v_{11} = 0$ particles. These
waves will be strongly damped by the thermal electrons, and since the
diffusion coefficient is proportional to the spectral wave energy,
$D(\alpha) \simeq |\Omega_-| \left(\frac{B_K}{B}\right)^2$, the diffusion coefficient, $D(\alpha) \simeq 0$ when $\omega \simeq |\Omega_-|$.
Consequently, particles with near 90° pitches only weakly interact with
whistlers and therefore their lifetimes are long. (Note that their life-
times are not infinite since 90° pitch particles can be scattered in pitch-
angles by the bounce resonance mechanism provided a suitable wave spectrum
exists (Roberts and Schulz, 1968)). The important conclusion is that 90°
pitch particles have longer lifetimes than particles with pitches < 90°.
Since $\alpha < 90°$ particles are rapidly diffusing toward the loss cone and gaining
energy (recall that we are near strong diffusion), the quantity $J(\alpha < 90°)/J(\alpha = 90$
should initially decrease with time. Therefore, the anisotropy factor, A,
increases. The anisotropy A should finally return back to the equilibrium

value after a time of the order of the lifetimes of 90° pitch particles. These qualitative arguments presented above can account for the observed similarities in the precipitation and trapped flux-time profiles as well as the pitch-angle anisotropy behavior. We note that in strong pitch-angle diffusion, the acceleration and precipitation are strongly coupled. The acceleration and pitch-angle diffusion times are related through $T_E \simeq T_\alpha (E/E_C)^2$ where T_α and T_E are pitch-angle diffusion and acceleration times, E is the energy, and E_C the critical energy, $B^2/8\pi N$. In the outer radiation zones, whistler wave amplitudes in the equatorial plane are often as large as 70 milligammas during substorms. (Brody et al., 1969; Russell et al., 1969). If 50 milligamma whistler field is used and assuming that $E/E_C \simeq 2$ ($E_C \simeq$ 20-30 keV in the outer zone) the corresponding acceleration time is about 10 minutes. If $E/E_C \simeq 1$, $T_E \simeq 200$ sec. This means that electrons can gain 20-30 keV energy in a few minutes of time during strong diffusion.

For the different behavior of $\simeq 50$ keV and $\simeq 150$ keV electrons, we note that according to the whistler theory (1) the minimum lifetime of electrons is $T_M = 2T_B/\alpha_o^2$, where T_B is the particle bounce time and α_o is the equatorial loss cone size. Therefore, the lifetimes of 50 keV and 150 keV particles differ by about 1.5, and consequently, the 150 keV electrons diffuse in pitch-angle and energy faster than the 50 keV electrons; (2) the 150 keV electrons resonate with not only the whistlers that they generate near the equatorial plane, but also with those generated by lower energy electrons off the equatorial plane, the latter effect arising from the change in the resonance condition for a given frequency whistler due to the increase of the magnetic field B off the equator. Consequently, the more energetic electrons should be accelerated to their maximum flux and attain diffusion equilibrium in less time than it takes for the lower energy electrons (a result consistent with observations).

The whistler interactions appear to affect predominantly the $\simeq 50$ keV electrons. There are at least two reasons why the ≥ 150 keV electrons are not affected as often. First, the ambient electron flux level at these energies is often well below the critical flux for self-generation of whistler waves. Consequently, the $\simeq 150$ keV electrons are affected mainly through whistler-mode turbulence generated by lower energy electrons. Second, since in whistler thoery the diffusion rate is proportional to the wave spectrum, very intense whistler waves are needed for particles to effectively diffuse in energy. Moreover, if available wave energy is limited, the acceleration at $\simeq 150$ keV energies may not be as effective as at $\simeq 50$ keV. By the same token, precipitation of high energy electrons should also be limited. Our precipitation measurements are not adequate to provide this information, but we note that O'Brien's (1964) observations are in agreement with the above conclusion.

Since the diffusion coefficient and the whistler wave spectrum are related by $D^* \simeq k^* \Omega_- \; (B_K/B_O)^2$, we can estimate the whistler wave amplitude near resonance. If the observed diffusion coefficient is used where $D^* \simeq 1/T_L = 10^{-3}$ (sec)$^{-1}$, and Ω_- is about 2×10^4 rad/sec, we get a wide-band wave intensity $B' \simeq 10^{-2}$ gammas if 100 gamma ambient flux value is used. Recent OGO-3 and OGO-5 observations (Russel et al., 1969; Brody et al., 1969) of whistler noise and chorus in the equatorial plane showed RMS values of $> 10^{-2}$ gammas. Finally, the growth rate is roughly $\Gamma \simeq \Omega_- \eta A$. The observed anisotropy (A) is about 1/3, Ω_- is about 2×10^4 rad/sec, and the number of resonant particles (η) present is about 3×10^{-3} (cm^3)$^{-1}$, giving a growth rate of about 20 rad/sec. This growth rate is roughly 10 times the growth factor for weak diffusion (Kennel and Petschek, 1966).

B.   A model of magnetospheric substorms for ≈ 50 keV electrons.

It has been known for some time that the intensity of electron fluxes observed at the ATS-1 orbit during magnetospheric substorms is local time dependent (Lezniak et al., 1968; Parks and Winckler, 1968). As was shown, the largest electron fluxes are observed between local midnight and local dawn. After local dawn, the peak electron fluxes attained become smaller and in the dusk to midnight sector, the peak fluxes are usually a factor of 4-5 smaller than those in the early morning sector. Parks and Winckler (1968) have interpreted the large degree of asymmetry in the electron production in terms of a large-scale magnetospheric acceleration process, the strength of acceleration being local time dependent. Inherent in this model is that the increases of electron fluxes observed by the ATS-1 during substorms are particles accelerated in the immediate vicinity of the satellite where measured (consistent with lifetime calculation shown in Table 1), and more-over, the precipitation represents a direct measure of freshly accelerated energetic electrons in the loss cone.

Recently, however, Pfitzer and Winckler (1969), Lezniak and Winckler (1969), and Arnoldy and Chan (1969) contested the above model and offered an alternative one. Lezniak and Winckler (1969) and Arnoldy and Chan (1969) comparing the ATS-1 detected electron fluxes with groundbased magnetic bays, and Pfitzer and Winckler (1969) correlating the ATS-1 detected electron fluxes with particle measurements on OGO-3 satellite as the satellite traversed the magnetosphere during substorms, concluded that the acceleration occurs in a small region centered around local midnight. According to these investigators, the increases of electron fluxes observed by the ATS-1 at

local times away from the midnight sector are particles initially injected near local midnight which under curvature and gradient forces have drifted to other local times where measured. They attribute the observed diminishing of electron fluxes at the ATS-1 orbit in local time to some particles being scattered into the loss cone while drifting in longitude, the scattering mechanism being the whistler resonance interaction (Kennel and Petschek, 1966).

These two models differ in (1) the spatial extent over which the acceleration occurs, and (2) what the precipitated particles represent. One of the main difficulties with the "small-scale" acceleration model is that it cannot adequately explain the intense auroral precipitation and the excellent correlation between precipitation and trapped electron flux-time profiles. Although the pitch-angle diffusion model (Kennel and Petschek, 1966) was invoked to account for the correlation between precipitated and trapped fluxes, it should be recognized that the weak pitch-angle diffusion mechanism cannot precipitate out particles fast enough to account for the intense auroral precipitation, since the weak diffusion rate corresponds to a particle "lifetime" of about 3×10^4 seconds, which is considerably longer than the substorm duration. On the other hand, if strong pitch angle diffusion is invoked, then one can precipitate out particles efficiently, but then the lifetime (2-300 seconds) is too short for particles to have drifted any appreciable distance. Consequently, if particles are injected in a small region near midnight, one must seek another mechanism than pitch-angle diffusion to account for the precipitation.

There is yet another experimentally observable fact which does not bear out the "small-scale" acceleration model. To account for the excellent correlation between precipitated and trapped electron flux increases, the

model invoked some scattering mechanism. What this implies is that whenever one measures precipitated fluxes, one must also observe the precipitation region to move eastward with drift speeds. At ionospheric heights of about 100 km where most of the electrons lose all their energies, the drift speed for 40 keV electrons in a dipole field in the absence of electric field is about 1 km/second. Consequently, such motions can easily be detected by balloon borne-detectors. Beginning in 1964, complicated balloon payloads were designed by the Berkeley group with the primary purpose of finding just such motions in precipitation regions. The payloads included directional telescopes (Parks, 1967) and tri-centric telescopes (Parks et. al., 1968a). Out of 17 balloon flights which included over 20 substorm events, only one event showed evidence of an eastward motion (Parks, 1967). The observed motion was in the east-direction but the speed was about 250 meters/second, a factor of 4 slower than the drift speed for 40 keV electrons. (At present, there are on record exactly 3 events that showed any precipitation source motion. The event observed by Brown (1962) drifted in the east direction with a speed of about 300 m/second; the recent event observed by the French group (University of Toulouse) showed a southeast motion of about 250 meters/second). All others, aside from the rapid forms, showed essentially isotropic intensity distribution during precipitation. The precipitation measurements included all local time regions extending from near local midnight to several hours past local noon.

The numerous magnetospheric phenomena do not occur independently but show strong correlation with auroral disturbances. Studies of correlation between magnetospheric particles and fields and auroral disturbances indicate that possibly a single large-scale disturbance phenomenon is responsible for the numerous geophysical effects. For example, the 40 keV electron islands

(Anderson, 1965) which have now been observed as far as at the moon's orbit
. in the magnetotail region, are associated with auroral magnetic bays and
auroral substorms (Akasofu, 1964). Rothwell and Wallington (1967) have shown
that onset times of magnetic bays and 40 keV electron islands are delayed.
The delay times closely correspond to wave propagation times, rather than
particle streaming times. Rothwell and Wallington concluded that the 40
keV electrons in islands are accelerated to these energies by the interaction
of the outward propagating waves (presumably generated during substorms)
and plasmas in-situ wherever the satellites observe them. A similar conclusion
was arrived at by Retzler and Simpson (1969) who suggested that electrons
(including relativistic ≈500 keV electrons) in islands are accelerated locally
in and throughout the neutral sheet by some form of plasma instability.
Other correlated magnetospheric phenomena include (1) inward motion of plasma-
pause (Carpenter, 1966), (2) radial motion of plasma sheet (Vasyliunas, 1968),
(3) emission of magnetic micropulsations (McPherron, 1967), (4) energetic
electron precipitation, (5) emission of VLF noise (Morozumi, 1965) and
(6) collapse of high-latitude trapping boundary (Williams and Ness, 1966).
These correlated magnetospheric and auroral disturbances are ascribed to
Magnetospheric Substorms (Jelly and Brice, 1967; Parks et al., 1968a;
McPherron et al., 1968; Coroniti et al., 1968).

The substorm phenomena are correlated with the dynamics external to the
magnetosphere. Fairfield and Cahill (1966) and Rostoker and Falthammer (1967)
related the south-directed interplanetary magnetic field to occurrence of
auroral disturbances. Schatten and Wilcox (1967) showed that generally higher
K_p indices were observed when the interplanetary field direction was south-
ward. Finally, Arnoldy and Chan (1969) indicated that although substorm

related features could not be found in the solar wind data, abrupt pressure increases in solar wind were observed preceeding a series of magnetospheric substorms.

Although we are ignorant of the detailed mechanisms, it is our contention that numerous forces within and external to the magnetosphere act collectively to trigger a macroscopic instability and produce the extensive correlated magnetospheric and auroral effects. It is possible that the solar wind and the magnetosphere are coupled by the field line merging process (Dungey, 1963; Levy et al., 1964; Axford et al., 1965). The subsequent reconnection of these field lines in the tail region will bring in solar wind energy and plasma into the magnetosphere. Some plasma particles, in transit, are probably accelerated to a few kilovolts by the convective flow from the neutral sheet to the nightside auroral zone. The influx of new plasmas and kilovolt particles alters the physical dynamics and the distribution of the ambient magneto-plasma medium. As more and more particles and plasmas are brought into the magnetosphere, the magnetosphere will reach a state when it cannot sustain further changes, leading to catastrophic release of stored energy in various forms. The process does not end here: because complicated waves and energetic particles are generated, these waves and particles can couple giving rise to numerous microscopic plasma instabilities, causing possibly further particle acceleration and modulation. The various periodic structures in precipitated fluxes and the correlated structures in micropulsations are probably results of these micro-instabilites. Consequently, the various temporal forms observed at different local times may be interpreted as local time characteristics of the world-wide magnetsopheric substorm.

We conclude by showing a schematic diagram illustrating the world-wide region over which energetic particles are produced in the magnetosphere during substorms (Figure 30). From precipitation measurements, one deduces that the latitude regions covered by the 50 keV electrons to extend out from about plasma pause (L = 4), to past L = 8 region, covering generally the "trough" region of the magnetosphere. In longitude, the $\approx$50 keV electrons cover the entire magnetosphere, but the intensity varies in local time. We believe the strength of the acceleration is strongly a function of the local time, with the maximum strength covering a broad region from about midnight to local dawn. After dawn, the strength diminishes slowly and the minimum (as deduced from electron production intensities) is observed between dusk and midnight.

Acknowledgements

Table 1. Lifetimes of Substorm Electrons

.

Date	Average Equatorial Electron Flux	Average Auroral Precipitated Electron Flux	Lifetime
April 2, 1967	$8 \times 10^6 (cm^2\text{-sec-ster})^{-1}$	$10^6 (cm^2\text{-sec-ster})^{-1}$	1930 sec
April 19, 1967	4×10^6	10^6	970
	5×10^6	10^6	1200
April 21, 1967	8×10^6	1.6×10^6	1300
August 11, 1967	6×10^6	7×10^6	200
	3×10^6	3.5×10^6	200
August 17, 1967	6×10^6	10^6	1400

Figure Captions

Figures 1 to 4:   Simultaneous recordings of trapped electron flux variations

at the geostationary orbit and precipitation fluxes near the

satellite magnetic conjugate in the auroral zone. Note that

the correlation is extremely good in the local time sectors

≈0400-1400 hours. The cosmic background in balloon X-rays

for Figures 2-4 is ≈80 counts/sec. UT = 150° WMT + 10 hours.

For detailed descriptions of the individual events, see text.

Figure 5:   Simultaneous measurements of particle fluxes between

≈1500-1900 local hours. The two time profiles begin to lose

correlation in these local times.

Figure 6:   Simultaneous particle measurements between 1900-2300 local

hours. Here the two measurements appear totally uncorrelated.

Figures 7 and 8:   These show typical riometer absorptions recorded from L = 3.9

to L = 8.0 during increases of electrons observed at ATS-1

orbit. The precipitation is extended in the L region.

Figure 9:   Intensity of magnetic H component vs. time at the ATS orbit

for periods when energetic particle increases were observed.

Figures 10 to 14:   1-minute averages of equatorial electron count rates in all

ATS-1 electron energy channels. If the counts/sample in the

500-1000 keV channel are < 0.1, they are omitted from the figures.

Note that acceleration is predominant in 50-150 keV. For a

description of individual events, see text.

Figure 15:   ATS-1 counts (1-minute averages) in 3 energy ranges. Note

the simultaneous decrease of electron fluxes at ≈2300 UT.

This effect is due to L-shell distortion.

Figure 16:   ATS-1 counts (1-minute averages) in 3 energy ranges. The

                  variations in 150-500 and 500-1000 keV are adiabatic variations.

                  The variations in 50-150 keV are a combination of both adiabatic

                  and non-adiabatic changes.

Figure 17:   Schematic diagram showing detector orientation on spacecraft

                  from which pitch-angles are calculated.

Figures 18 to 23: Examples of equatorial electron pitch-angle distributions for

                  50-150 keV and 150-500 keV energy channels at various substorm

                  stages. The data represent pitch-angles averaged over 6° interva

                  and fluxes over 72 seconds. Note that pitch-angle distributions

                  are peaked toward 90°. See text for individual descriptions.

Figure 24:   Pitch-angle distribution at various times for the event shown

                  in Figure 15. Note that in both 50-150 keV and 150-500 keV

                  energies, the distributions change drastically during L-shell

                  modulation. Note that the distributions of 150-500 keV peak

                  toward smaller pitches between 2335 and 2339 UT.

Figures 25 and 26: 72-second averages of ATS-1 count-rate vs. time profiles

                  together with anisotropy vs. time profiles for the April 19

                  and April 21, 1967 event. Note the general similarities in the

                  two curves. Anisotropy increases with increasing electron fluxe

Figure 27:   Here is shown flux-time and anisotropy-time profiles of

                  150-500 keV electrons during substorms. Note the general

                  similarities in the two curves.

Figure 28:   Shows 72-second averages of count-rate vs. time together with

                  pitch-angle anisotropy vs. time profile. Note that while

                  50-150 keV anisotropy decreased, the 150-500 keV anisotropy

                  increased.

Figure 29:   Shows 1-minute averages of count-rate vs. time together

with pitch-angle anisotropy vs. time profile. Note that

the anisotropy is sometimes below zero, indicating that

pitch-angle distribution is ·peaked toward smaller pitches

than 90°.

Figure 30:   Shows a schematic diagram of 50 keV acceleration region in

the magnetosphere. The acceleration strength is local time

dependent.

References

Akasofu, S.-I., The Development of Auroral Substorms, Planetary and Space Sci., 12, 273, 1964.

Anderson, K. A., Energetic Electron Fluxes in the Tail of the Geomagnetic Field, J. Geophys. Res., 70, 4741, 1965.

Anderson, K. A. and D. E. Enmark, Balloon Observations of X-rays in the Auroral Zone II, J. Geophys. Res., 65, 3521, 1960.

Anderson, K. A. and D. W. Milton, Balloon Observations of X-Rays in the Auroral Zone, 3, High Time Resolution Studies, J. Geophys. Res., 69, 4457, 1964.

Arnoldy, R. L. and K. W. Chan, Particle Substorms Observed at the Geostationary Orbit, Univ. of New Hampshire report (1969); also, Trans, Am. Geophys. Union, 50, April, 1969 (abstract).

Axford, W. I. and C. O. Hines, A Unifying Theory of High-Latitude Geophysical Phenomena and Geomagnetic Storms, Can. J. Phys. 39, 1433, 1961.

Axford, W. I., H. E. Petschek and G. L. Siscoe, Tail of the Magnetosphere, J. Geophys, Res., 70, 1231, 1965.

Axford, W. I. Magnetospheric Convection, Rev. of Geophys. 7, 421, 1969.

Barcus, J. R. and T. J. Rosenberg, Energy Spectrum for Auroral-Zone X-Rays, 1, Diurnal and Type Effects, J. Geophys. Res., 71, 803, 1966.

Bethe, H. and J. Askin, in Experimental Nuclear Physics (E. Segre, Editor) 1, 166, New York, 1963.

Brody, K. I., C. T. Russel, R. E. Holzer, C. F. Kennel, R. W. Fredricks, and F. L. Scarf, Nightside Auroral Electric and Magnetic Noise in the Equatorial Plane (Abstract), Trans. Am. Geophys. Union, 50, April, 1969.

Brown, R. R., West-East Motion of an Auroral Zone X-Ray Event, J. Geophys. Res., 67, 31, 1962.

Brown, R. R., J. R. Barcus and N. R. Parsons, Balloon Observations of Auroral Zone X-Ray Pulsations, J. Geophys, Res., 70, 2599, 1965.

Carpenter, D. L., Whistler Studies of the Plasma-Pause in the Magnetosphere, 1, Temporal Variations on the Position of the Knee and Some Evidence on Plasma Motions Near the Knee, J. Geophys. Res., 71, 693, 1966.

Cornwall, J. M., Diffusion Processes Influenced by Conjugate Point Wave Phenomena, Radio Science, 3, 740, 1968.

Coroniti, F. V., R. L. McPherron and G. K. Parks, Studies of the Auroral Substorm, 3, Concept of the Magnetospheric Substorm and Its Relation to Electron Precipitation and Micropulsations, J. Geophys. Res. 70, 1715, 1968.

Cummings, W. D., J. N. Barfield and P. J. Coleman, Jr., Magnetospheric Substorms Observed at the Synchronous Orbit, J. Geophys. Res. 73, 6687, 1968.

Dungey, J. W., Interactions of Solar Plasma with the Geomagnetic Field, Planetary Space Sci. 10, 233, 1963

Evans, D. S., A 10-cps Periodicity in the Precipitation of Auroral-Zone Electrons, J. Geophys. Res. 72, 4281, 1967.

Evans, R. D., The Atomic Nucleus, McGraw-Hill, New York, 1955.

Falthammer, C.-G., Effects of Time Dependent Electric Fields on Geomagnetically Trapped Radiation, J. Geophys. Res. 70, 2503, 1965.

Fairfield, D. H., and L. H. Cahill, Transition Region Magnetic Field and Polar Magnetic Disturbances, J. Geophys. Res. 71, 155, 1966.

Frank, L. A., A Survey of Electrons > 40 keV Beyond 5 Earth Radii with Explorer 14, J. Geophys. Res. 73, 6189, 1965.

Hess, W. N., The Radiation Belt and Magnetosphere, Blaisdell, Waltham, Mass. 1968.

Hudson, H. W., G. K. Parks, D. W. Milton and K. A. Anderson, Determination of the Auroral Zone X-Ray Spectrum, J. Geophys, Res. 70, 4979, 1965.

Jelly, D. and N. Brice, Changes in the Van Allen Radiation Associated with Polar Substorms, J. Geophys, Res. 72, 5919, 1967.

Kennel, C. F. and H. E. Petschek, Limit on Stably Trapped Particle Fluxes, J. Geophys, Res. 71, 1, 1966.

Kennel, C. F., Consequences of Magnetospheric Plasma, Rev. of Geophys. 7, 379, 1969.

Lampton, M., Daytime Observation of Energetic Auroral-Zone Electrons, J. Geophys. Res. 72, 5817, 1967.

Lanzerotti, L. J., C. S. Roberts and W. L. Brown, Temporal Variations in the Electron Flux at Synchronous Altitudes, J. Geophys. Res., 72, 5893, 1967.

Levy, R. H., H. E. Petschek and G. L. Siscoe, Aerodynamic Aspects of the Magnetospheric Flow, AIAA J., 2, 12, 1964.

Lezniak, T. W., R. L. Arnoldy, G. K. Parks, and J. R. Winckler, Measurement and Intensity of Energetic Electrons at the Equator at 6.6 R_e, Radio Science 3, 710, 1968.

Lezniak, T. W. and J. R. Winckler, Magnetospheric Substorm Effects on Energetic Electrons in the Outer Van Allen Belt, University of Minnesota Cosmic Ray Technical Report CR-137, April (1969) to be published.

McDiarmid, I. B. and E. E. Budzinski, Angular Distributions and Energy Spectra of Electrons Associated with Auroral Events, Can. J. Phys. 42, 2048, 1964.

McDiarmid, T. B., J. R. Burrows and M. D. Wilson, Morphology of Outer Radiation Zone Electron (E > 35 keV) Acceleration Mechanisms, J. Geophys. Res. 74, 1749, 1969.

McPherron, R. L., Relation of Auroral Zone Micropulsations to Magnetospheric Substorms, Ph.D. Thesis, University of California, Berkeley (1967).

McPherron, R. L., G. K. Parks, F. V. Coroniti, and S. H. Ward, Studies of Magnetospheric Substorms, 2, Correlated Magnetic Micropulsations and Electron Precipitation Occurring During Auroral Substorms, J. Geophys. Res. 73, 1697, 1968.

Morozumi, H. M., Diurnal Variation of Auroral Zone Geophysical Disturbances, Rept. Ionospheric Space Res. Japan 19, 286, 1965.

Mozer, F. S. and R. Serlin, Magnetospheric Electric Field Measurements with Balloons, Space Sciences Laboratory Report, University of California, Berkeley, 1969.

Mozer, F. S. and P. Bruston, Auroral Zone Proton-Electron Anticorrelations, Proton Angular Distributions, and Electric Fields, J. Geophys. Res. 71, 4461, 1966.

O'Brien, B. J., Lifetimes of Outer Zone Electrons and Their Precipitation into the Atmosphere, J. Geophys. Res., 67, 3687, 1962.

O'Brien, B. J., High-Latitude Geophysical Studies with Satellite Injun 3, 3, Precipitation of Electrons into the Atmosphere, J. Geophys. Res., 69, 13, 1964.

Oliven, M. M. and D. A. Gurnett, Microburst Phenomena, 3, An Association Between Microbursts and VLF Chorus, J. Geophys. Res., 73, 2355, 1968.

Parks, G. K., R. L. McPherron, F. V. Coroniti and K. A. Anderson, Studies of Magnetospheric Substorm, I, Characteristics of Modulated Energetic Electron Precipitation Occurring during Auroral Substorms, J. Geophys, Res., 73, 1685, 1968a.

Parks, G. K., Spatial Characteristics of Auroral-Zone X-Ray Microbursts, J. Geophys. Res., 72, 215, 1967.

Parks, G. K., R. L. Arnoldy, T. W. Lezniak and J. R. Winckler, Correlation of Energetic Electrons Between the Equator at 6.6 R_e and the Auroral Zone During Magnetospheric Substorms, Radio Science 3, 715, 1968b.

Parks, G. K., and J. R. Winckler, Acceleration of Energetic Electrons Observed at the Synchronous Altitude during Magnetospheric Substorms, J. Geophys. Res. 5786, 1968.

Parks, G. K. and J. R. Winckler, Simultaneous Observations of 5-15 Second Period Modulated Energetic Electron Fluxes at the Synchronous Altitude and the Auroral Zone, to be published J. Geophys, Res., Aug., 1969.

Paulikas, G. A., J. B. Blake, S. C. Freden and S. S. Imamoto, Observations of Energetic Electrons at Synchronous Altitude, 1, General Features and Diurnal Variations, J. Geophys. Res., 73, 4915, 1968.

Perkins, F. W., Plasma-Wave Instabilities in the Ionosphere over the Aurora, J. Geophys. Res., 73, 6631, 1968

Pfitzer, K. A. and J. R. Winckler, Intensity Correlations and Substorm Electron Drift Effects in the Outer Radiation Belt Measured with the OGO-3 and ATS-1 Satellites, submitted to J. Geophys. Res. for publication, 1969.

Retzler, J. and J. A. Simpson, Relativistic Electrons Confined within the Neutral Sheet of the Geomagnetic Tail, J. Geophys. Res., 74, 2149, 1969.

Roberts, C. W. and M. Schulz, Bounce Resonant Scattering of Particles Trapped in the Earth's Magnetic Field, J. Geophys. Res., 73, 7361, 1968.

Rosen, L., G. K. Parks, J. R. Winckler and H. Sauer, The Latitude Distribution of Precipitation and its Relation to Substorm Increases in 50 keV Electrons at Synchronous Orbit, (abstract) Trans. Am. Geophys. Union 50, April 1969.

Rostocker, G., and C. G. Falthammer, Relationship Between Changes in the Interplanetary Magnetic Field and Variations in the Magnetic Field at the Earth's Surface, J. Geophys. Res. 72, 5853, 1967.

Rothwell, O., and V. Wallington, The Polar Substorm and Electron Islands in the Earth's Magnetic Tail, (preprint), paper presented at the Birkland Symposium, September, 1967.

Russel, C. T., R. E. Holzer, E. J. Smith, OGO-3 Search Coil Magnetometer Observations at the Geomagnetic Equator (Abstract) Trans. Am. Geophys. Union 50, April (1969).

Schatten, K. H., and J. M. Wilcox, Response of the Geomagnetic Activity Index Kp to the Interplanetary Magnetic Field, J. Geophys. Res. 72, 5185, 1967.

Swift, D. W., the Effect of Transverse Electric Fields on the Mirror Points of Charged Particles in the Magnetosphere, J. Geophys. Res. 70, 2529, 1965.

Vasyliunas, V. M., A Survey of Low-Energy Electrons in the Evening Sector of the Magnetosphere with OGO-I and OGO-III, J. Geophys. Res. 73, 2839, 1968.

Williams, D. J. and N. F. Ness, Simultaneous Trapped Electron and Magnetic Tail Field Observations, J. Geophys, Res. 71, 5117, 1966.

Winckler, J. R., P. D. Bhavsar, and K. A. Anderson, A Study of the Precipitations of Energetic Electrons from the Geomagnetic Field, J. Geophys. Res. 67, 397, 1962.
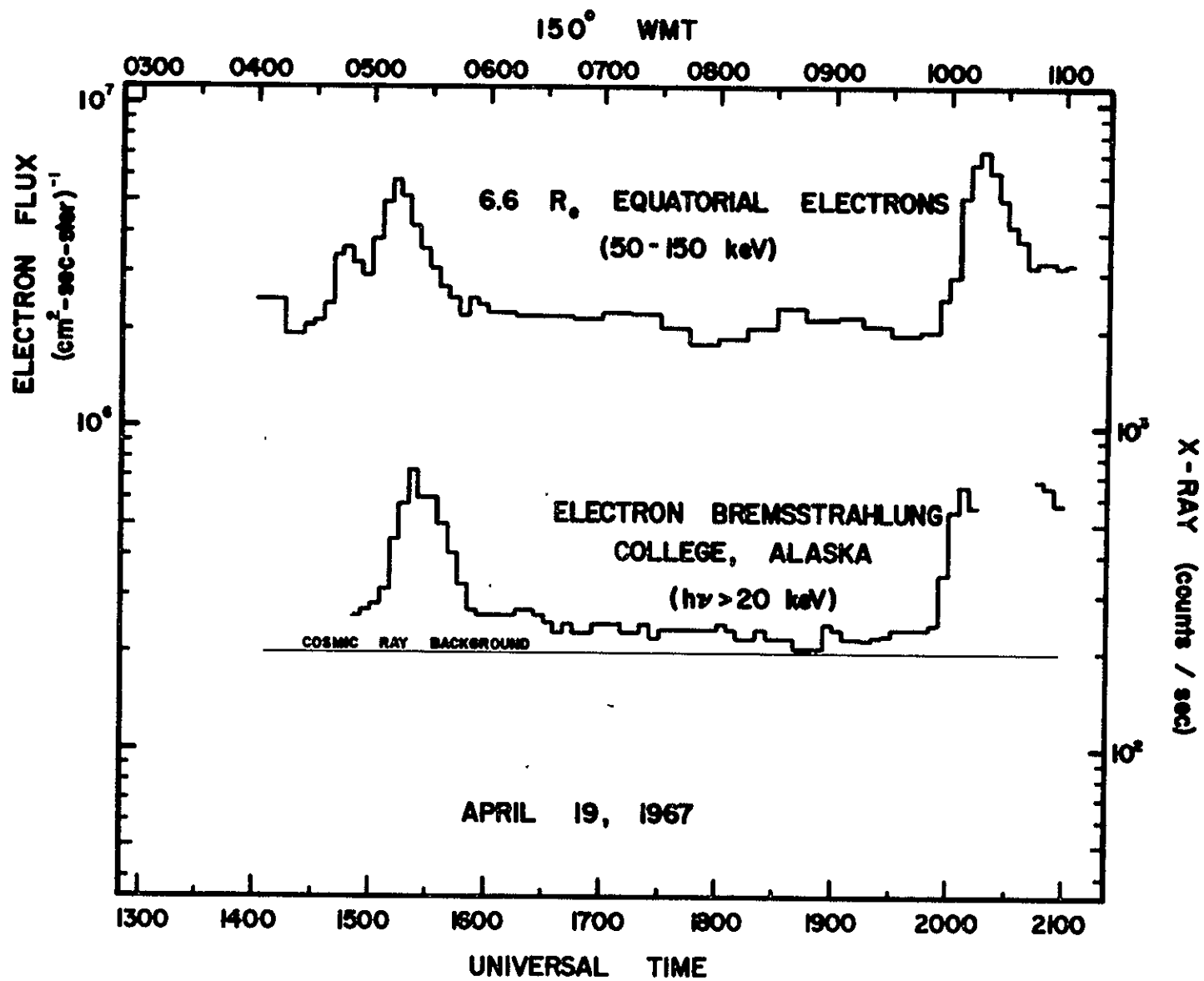
Figure 1
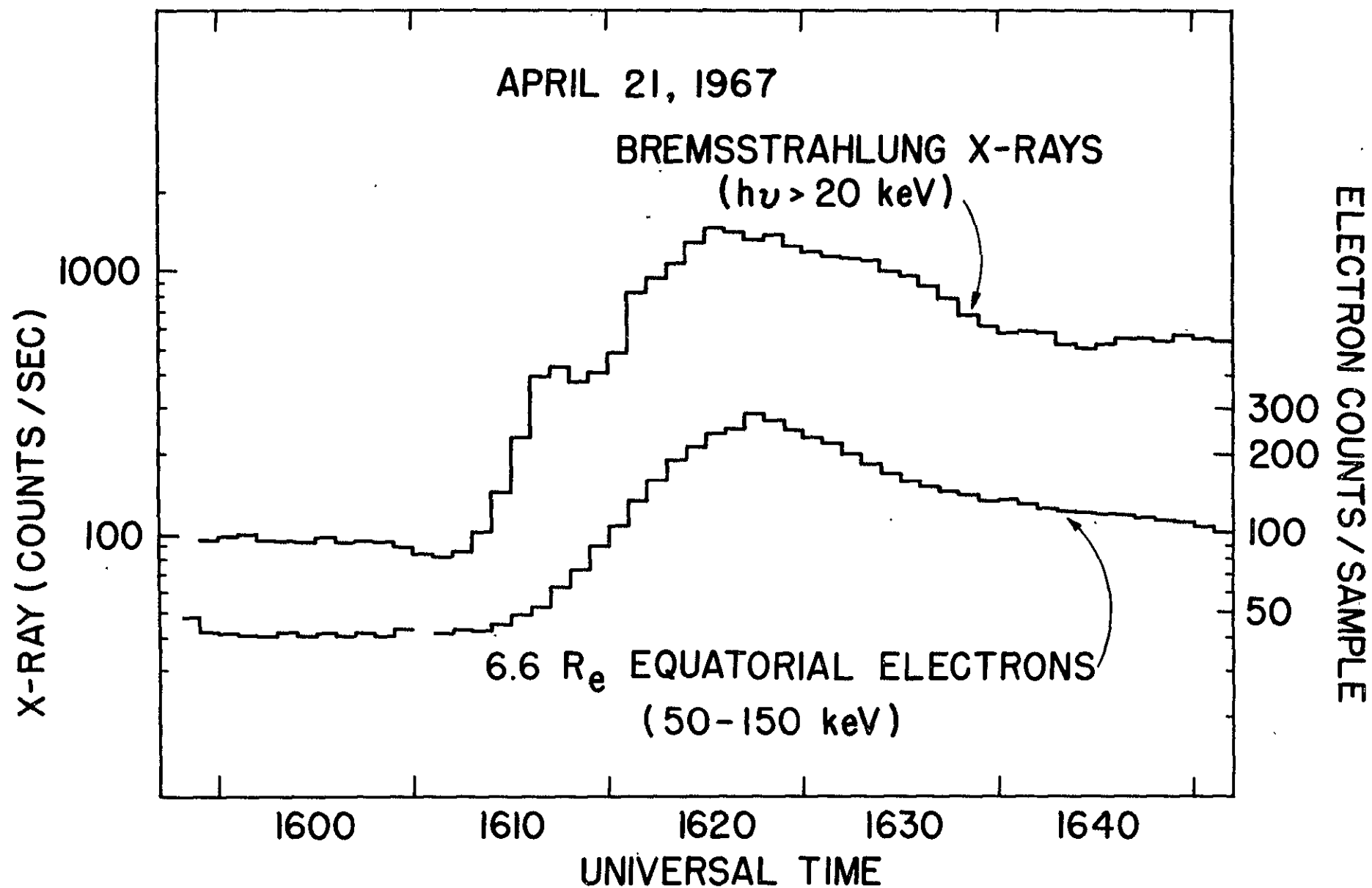
Figure 2
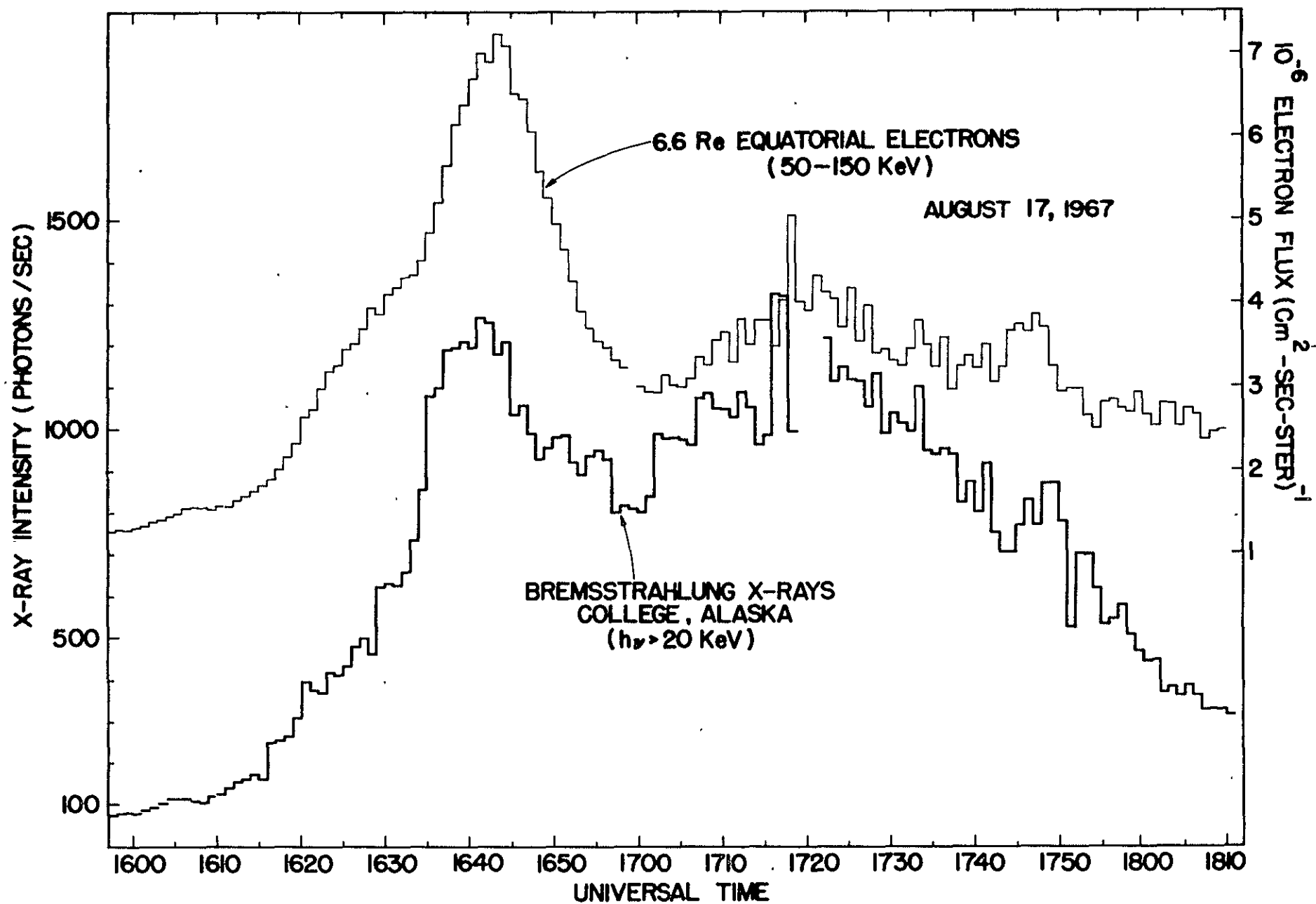
Figure 3

Figure 4

Figure 5

AUG 18, 1967
6.6 Re EQUATORIAL ELECTRONS
(50 < E < 150 keV)

AUG 18, 1967
BREMSSTRAHLUNG X-RAYS
COLLEGE, ALASKA
(hν > 20 keV)

AVERAGE ELECTRONS/SAMPLE

X-RAY INTENSITY (COUNTS/SECOND)

UNIVERSAL TIME
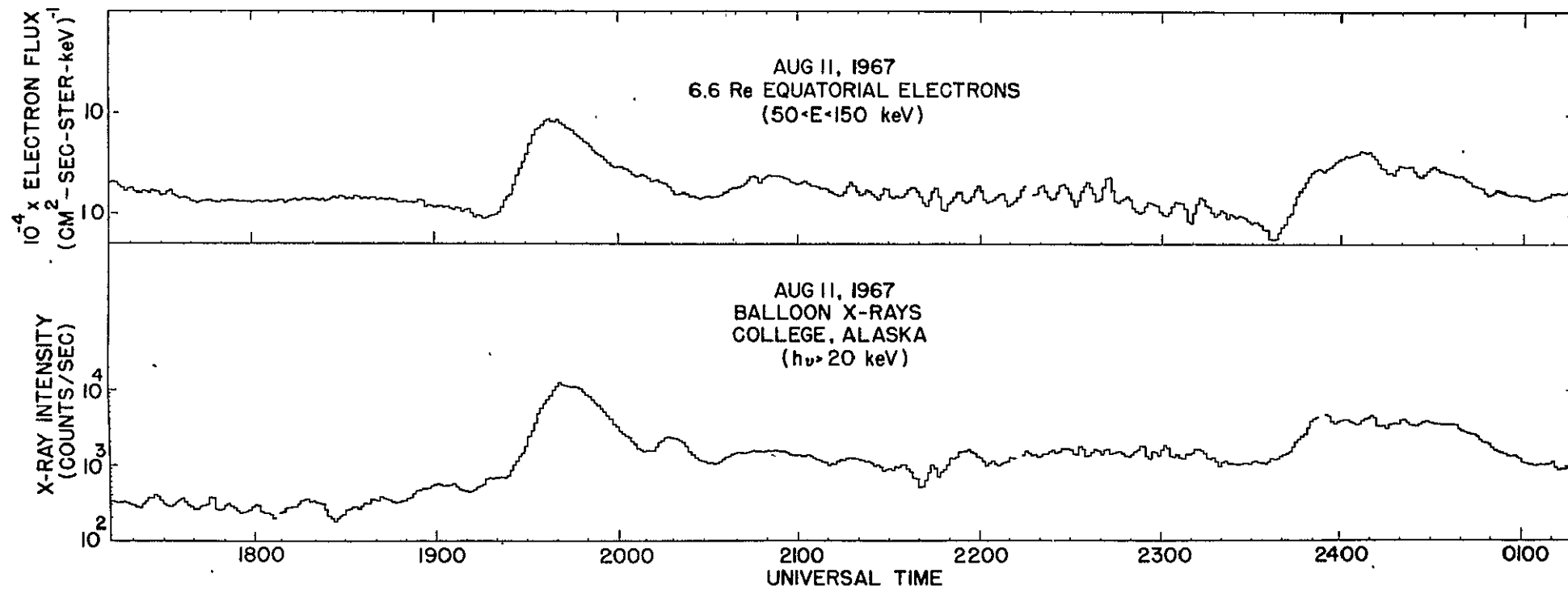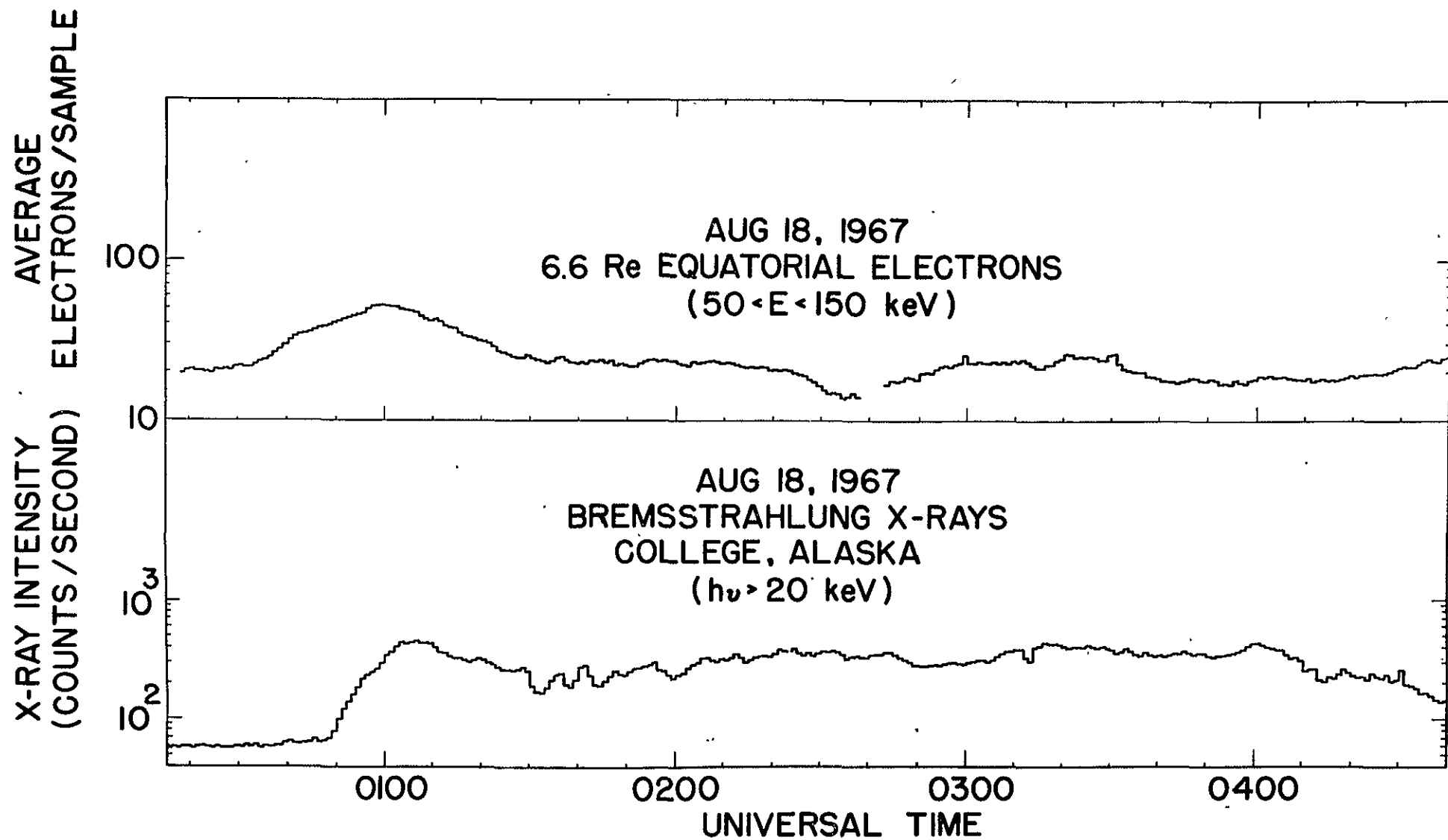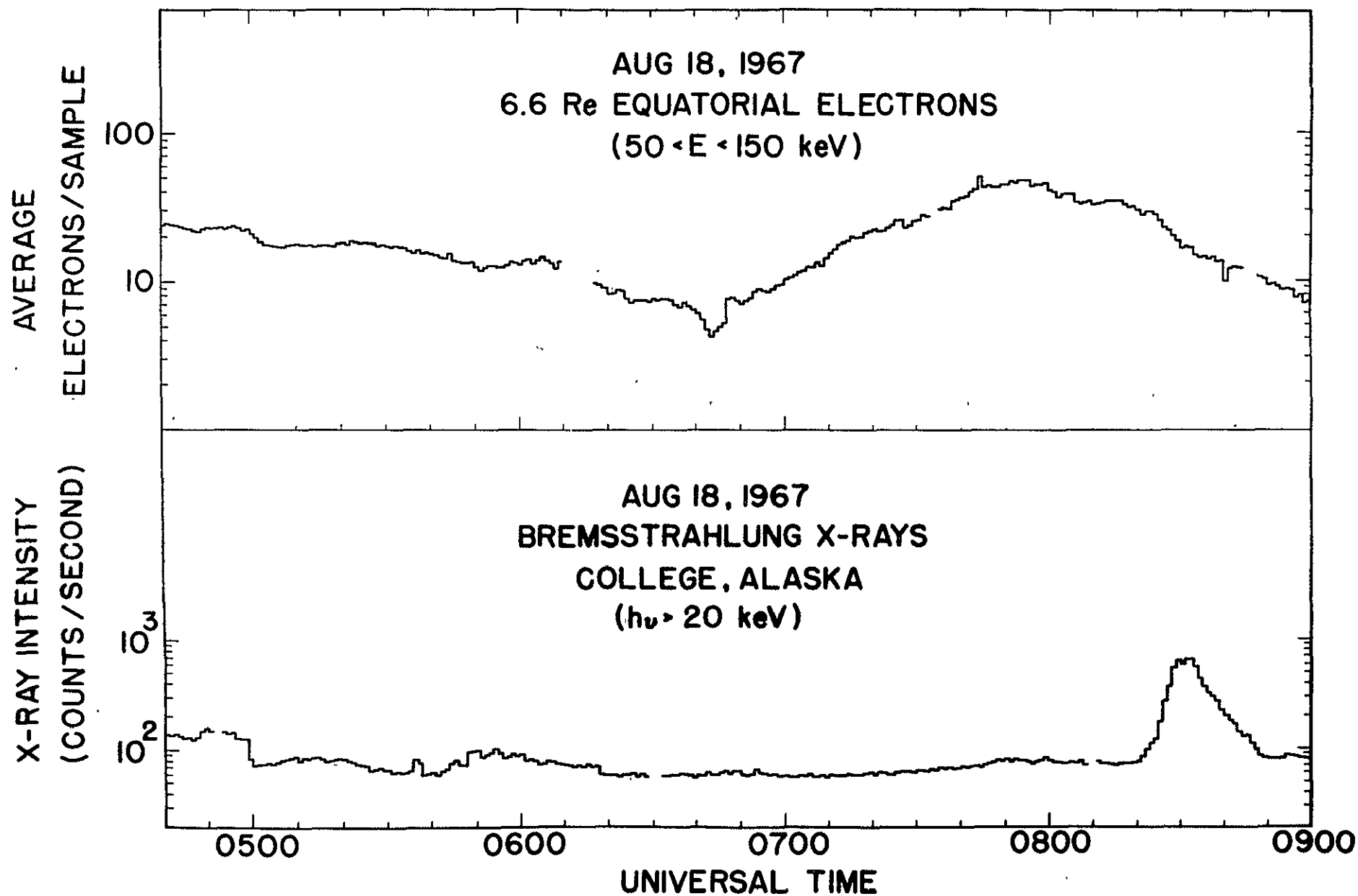
Figure 6

RIOMETER READINGS

L=3.9　　　　　WILDWOOD

L=4.2　　　　　ANCHORAGE

L=4.5　　　　　SHEEP MTN.

L=5.0　　　　　PAXSON

L=5.5　　　　　COLLEGE

L=6.3　　　　　FT. YUKON

L≈8.0　　　　　BARTER IS.

APRIL 2, 1967

10^7

10^6

10^5

200 γ

6.6 R_e EQUATORIAL
ELECTRONS
(50-150 keV)

COLLEGE MAGNETOMETER
H - COMPONENT

FLUX
(cm^2-sec-ster)$^{-1}$

1100　　　1200　　　1300　　　1400

UNIVERSAL TIME

Figure 7

RIOMETER (30 MHz)

WILDWOOD
L=3.9

ANCHORAGE
L=4.2

SHEEP MNT.
L=4.5

PAXSON
L=5.0

COLLEGE
L=5.5

FT. YUKON
L=6.3

BAR I
L=8.

ATS-B 50-150 KEV ELECTRONS

FLUX
$10^{-4} \times (cm^2\text{-sec-ster-keV})^{-1}$

10

5

0

1900   2000   2100   2200   2300

UNIVERSAL TIME (AUG. 11, 1967)
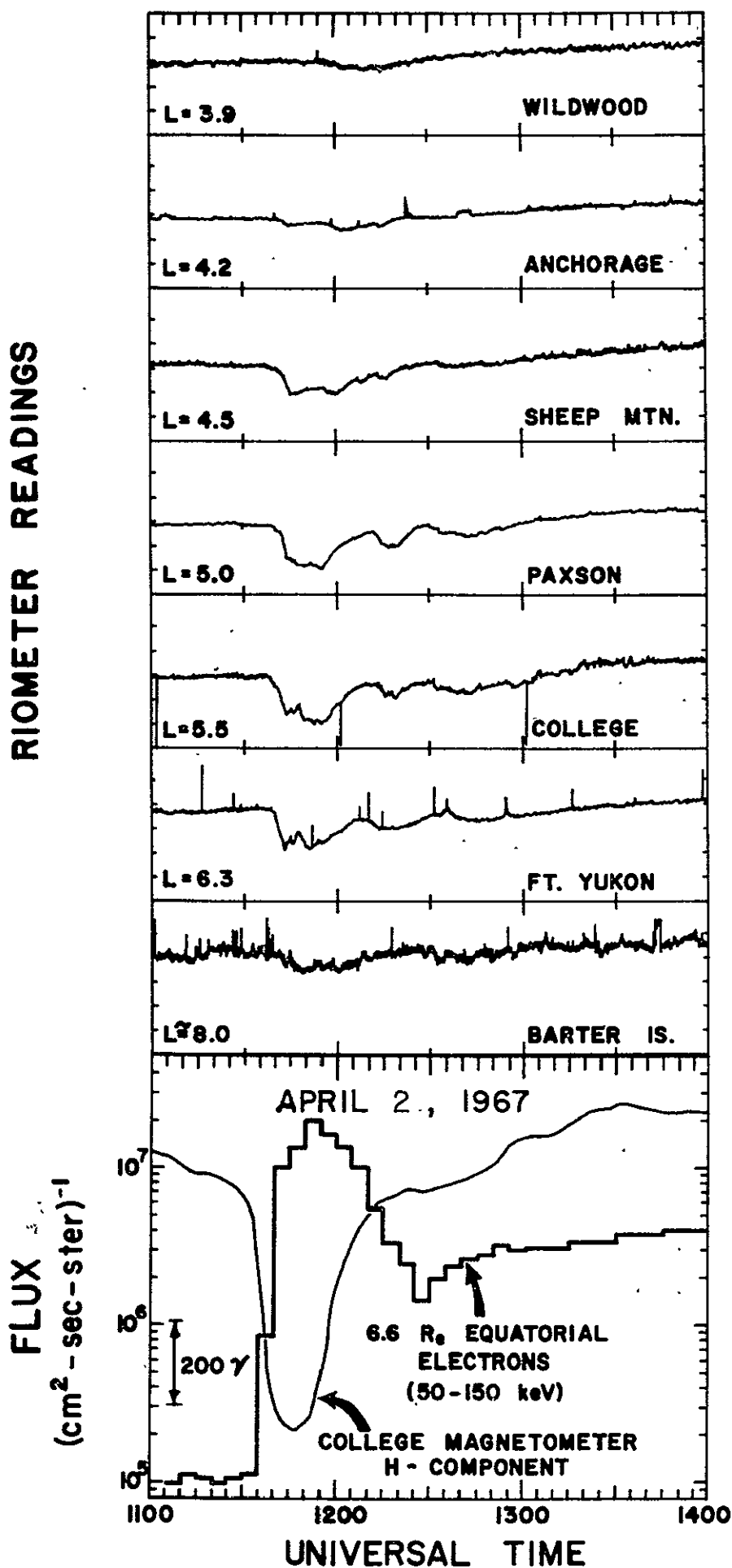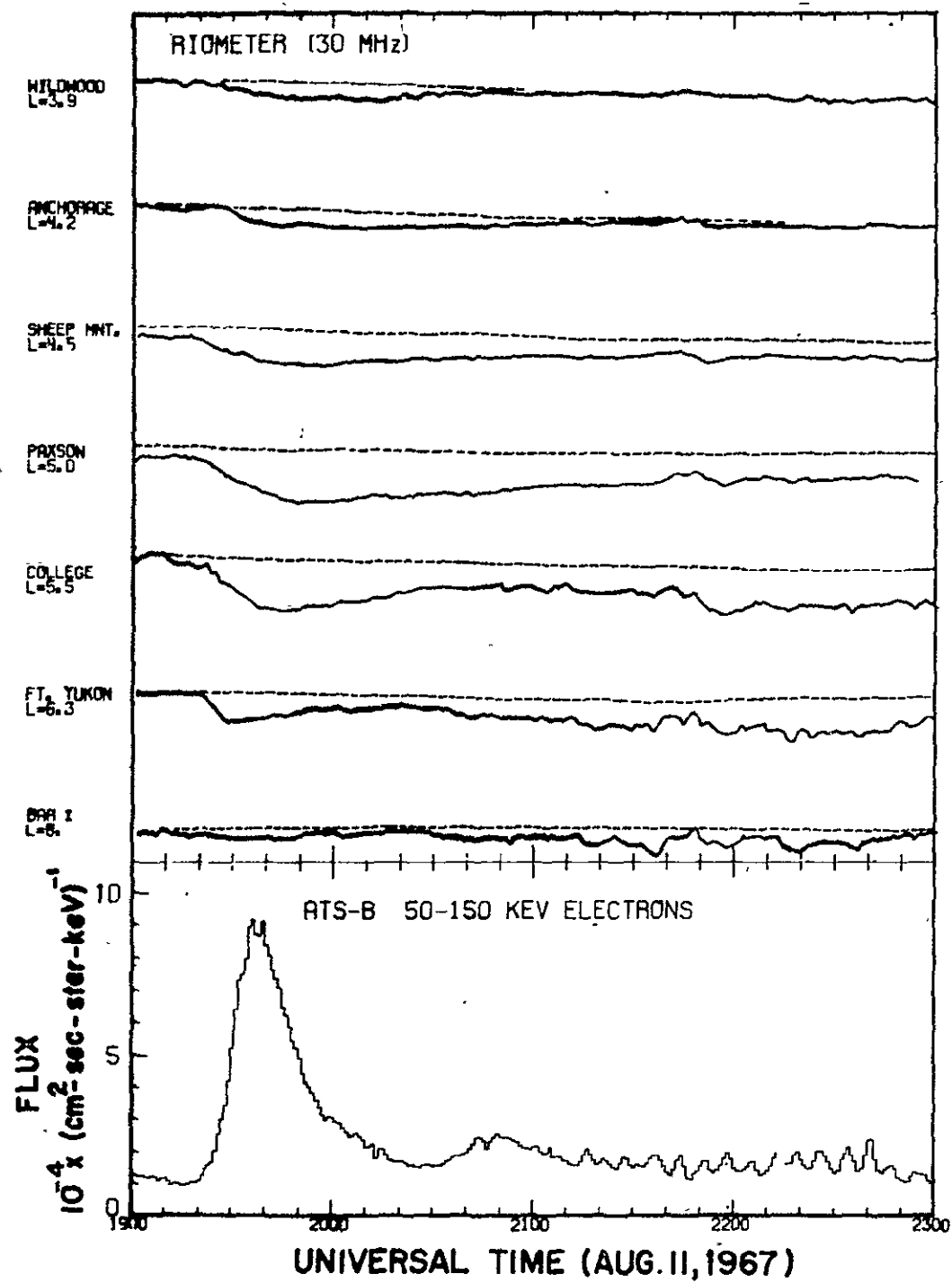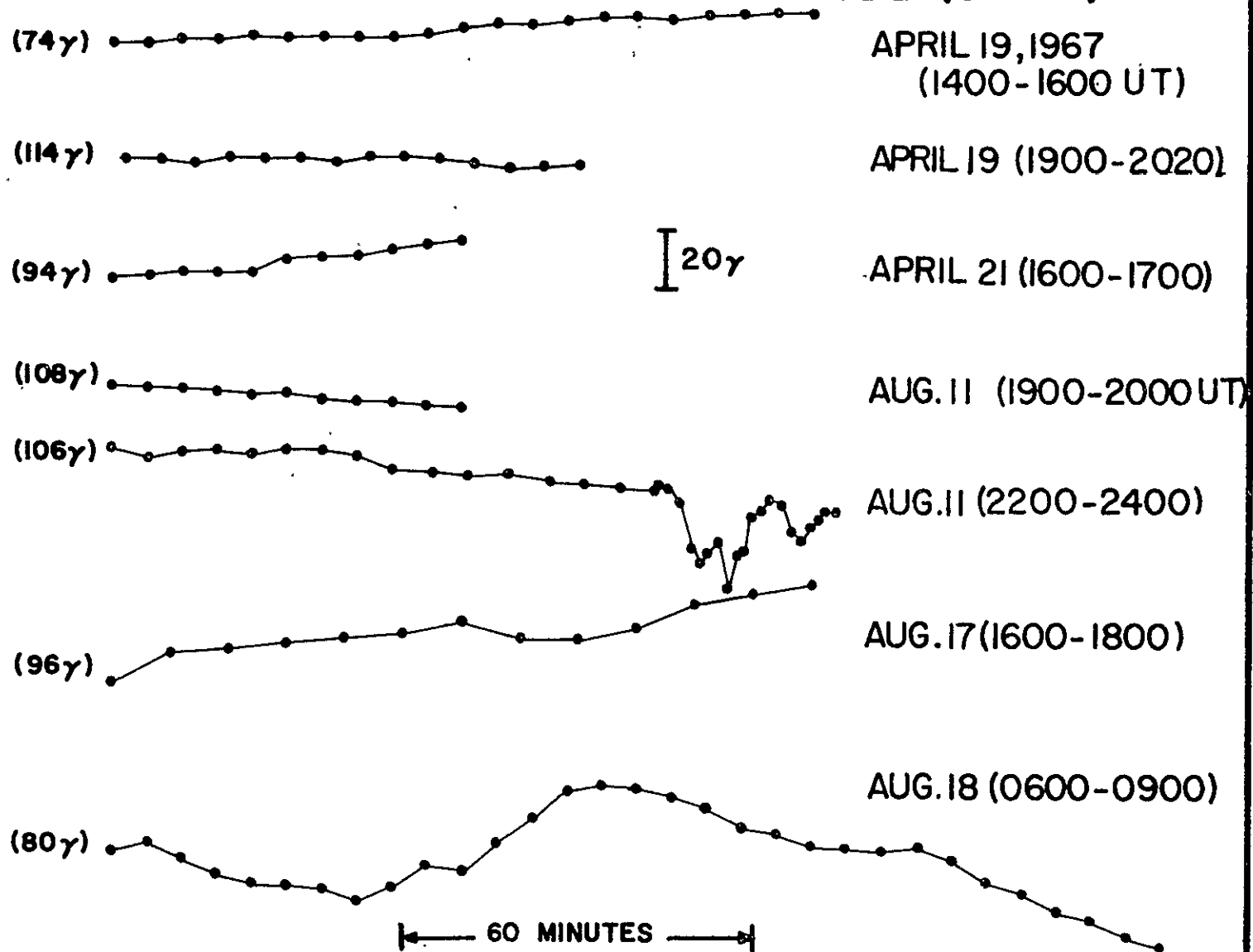
Figure 8

Figure 9

Figure 10

Figure 11

APRIL 21, 1967
ATS-1 ELECTRONS

50-150 keV

150-500 keV

500-1000 keV
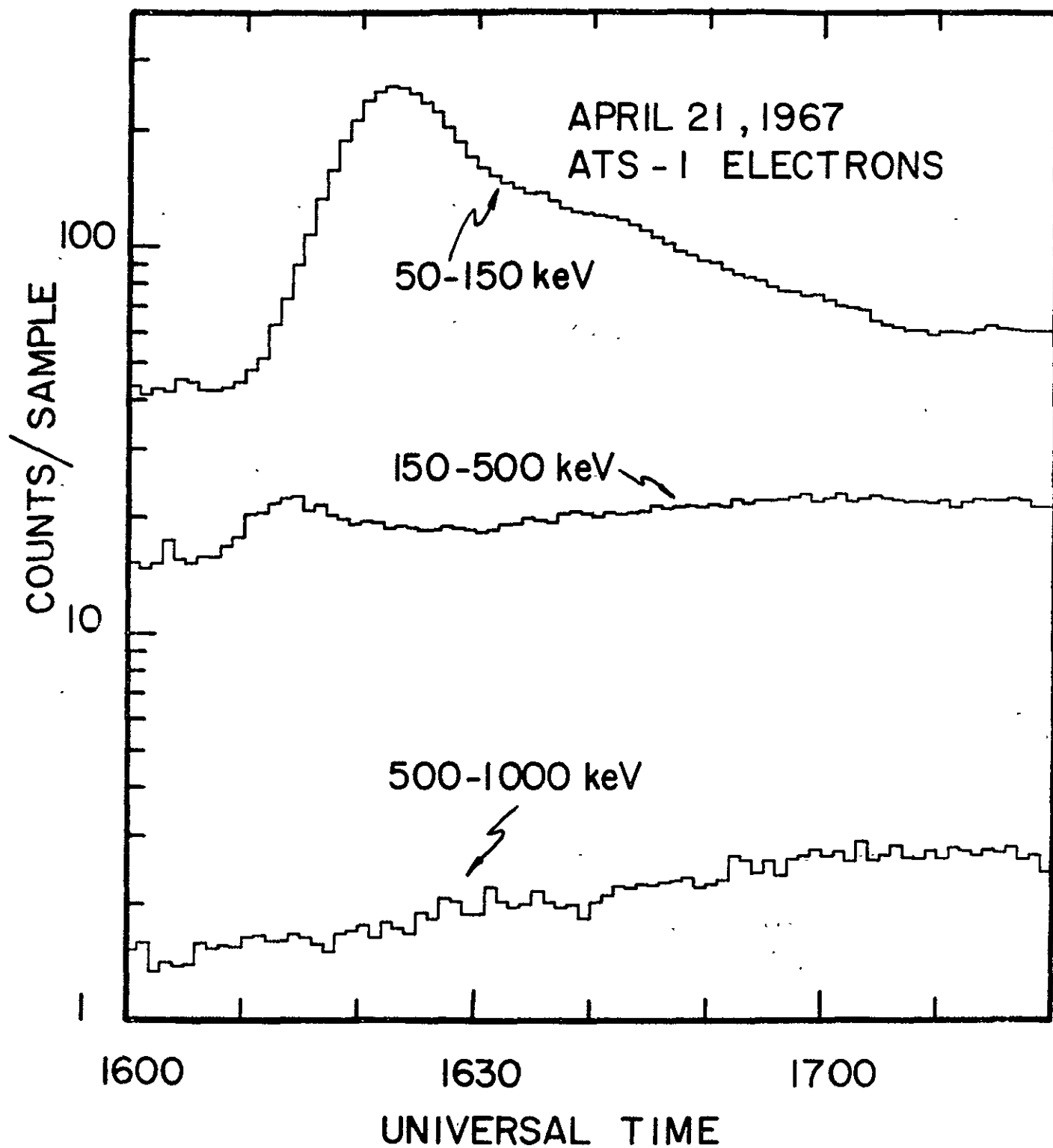
Figure 12

Figure 13

Figure 14

AUGUST 11-12, 1967

ATS-1 ELECTRONS

50-150 keV

150-500 keV

500-1000 keV

COUNTS/SAMPLE

100

10

UNIVERSAL TIME

2200   2330   2400   0030   0100

Figure 15

AUGUST 18, 1967
ATS-1 ELECTRONS

50-150 keV

150-500 keV

500-1000 keV

COUNTS/SAMPLE

UNIVERSAL TIME

Figure 16

−Z (SOUTH)

$\vec{-B}$

$\hat{d}$

α_{min} α_{max}

4°

N
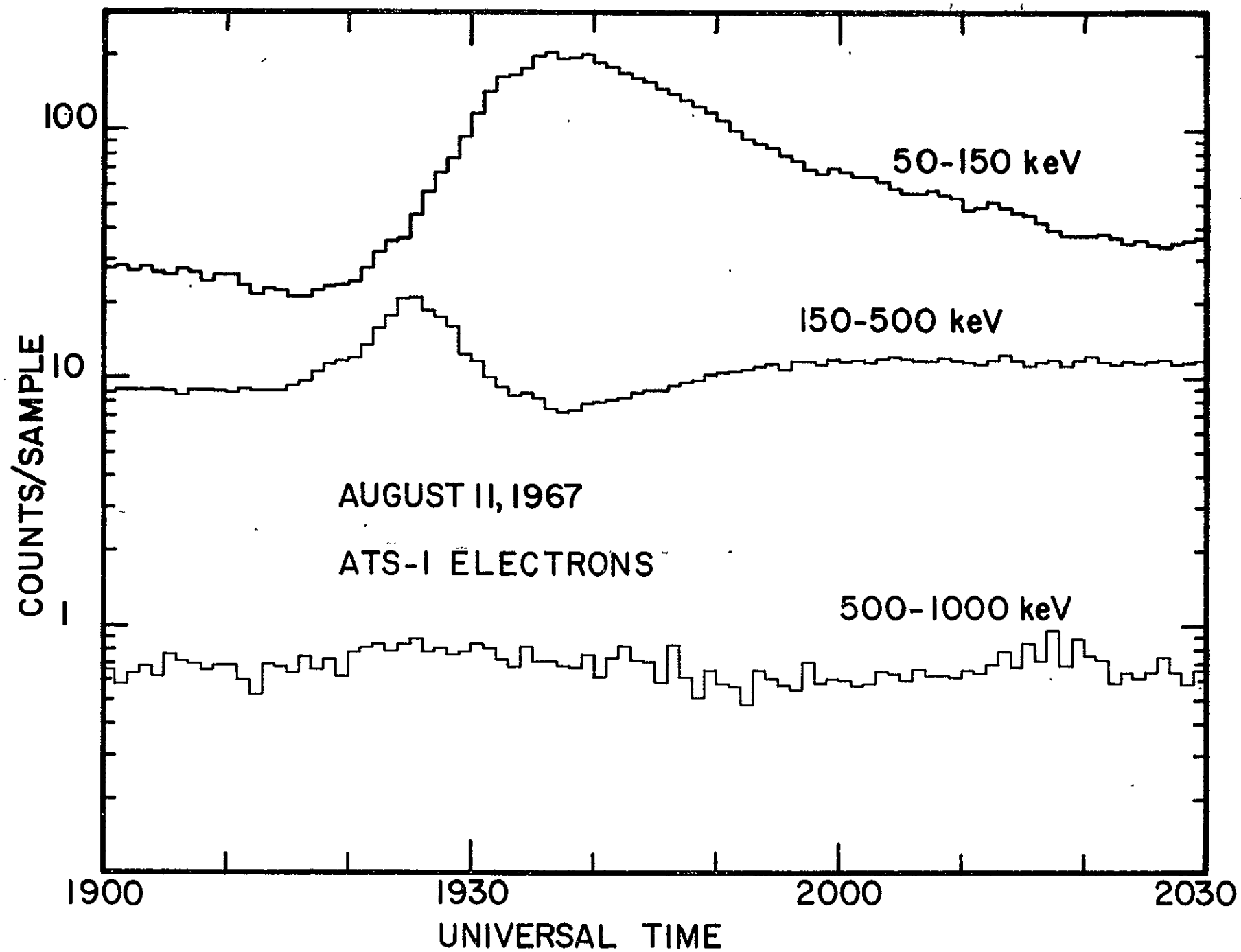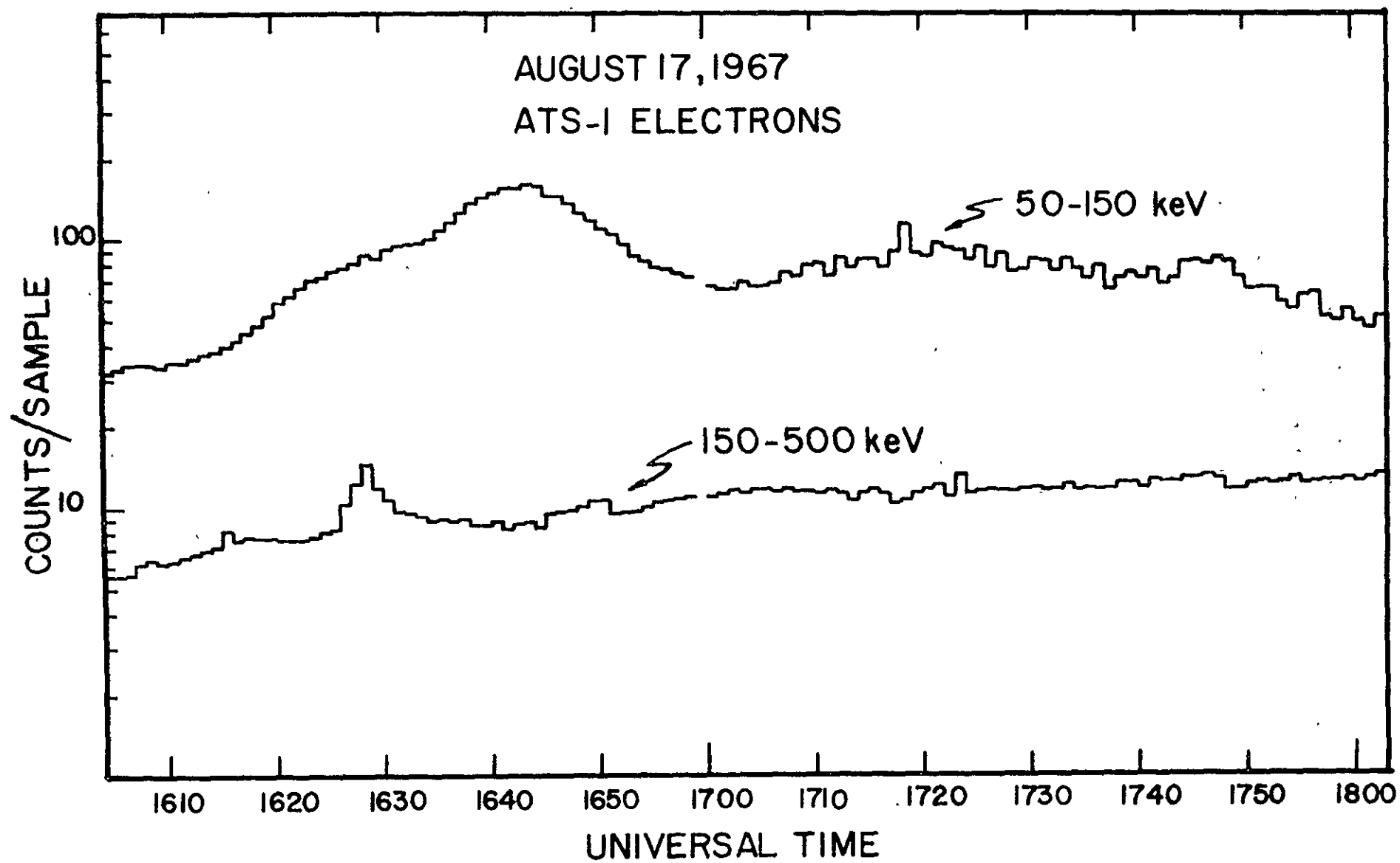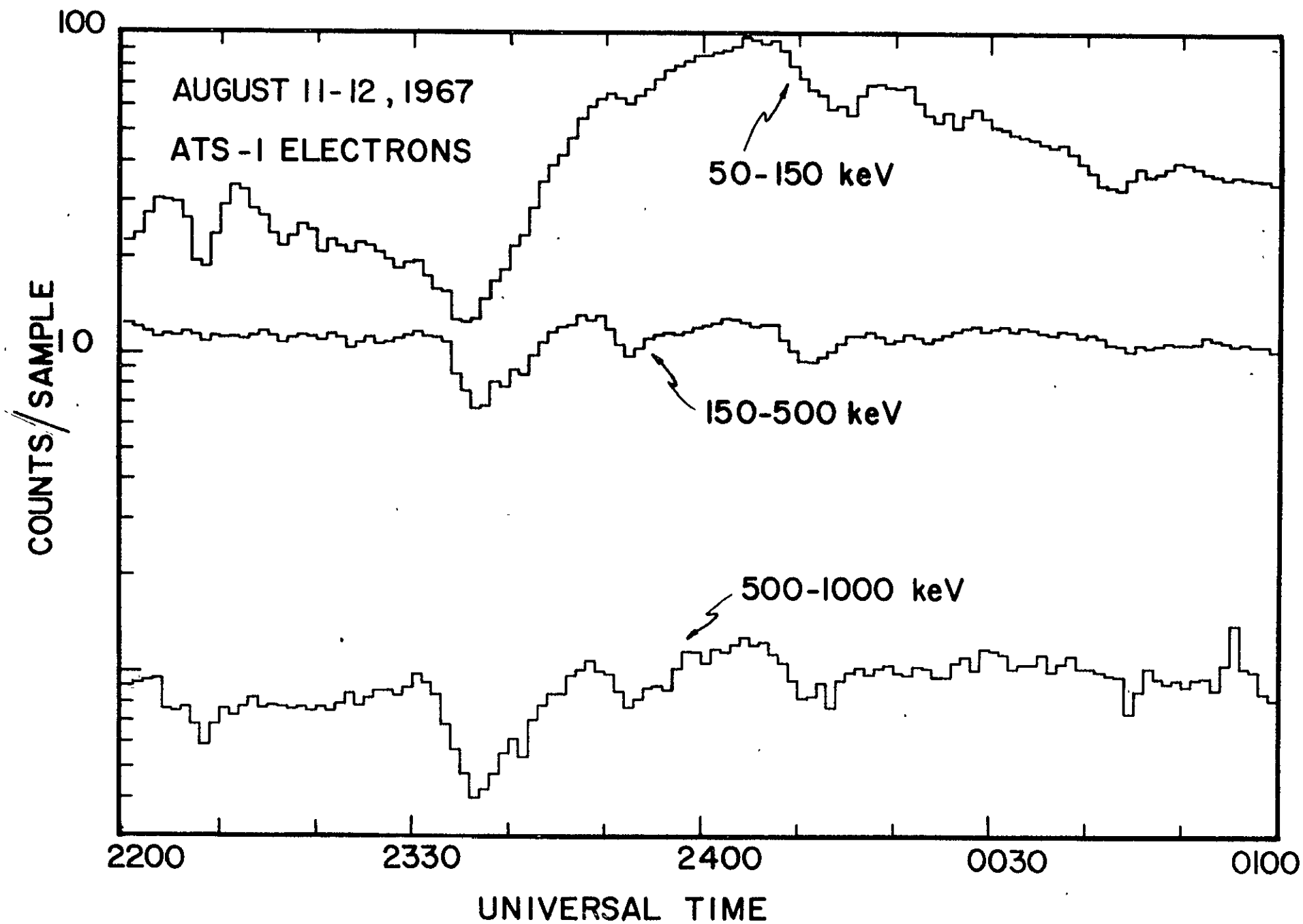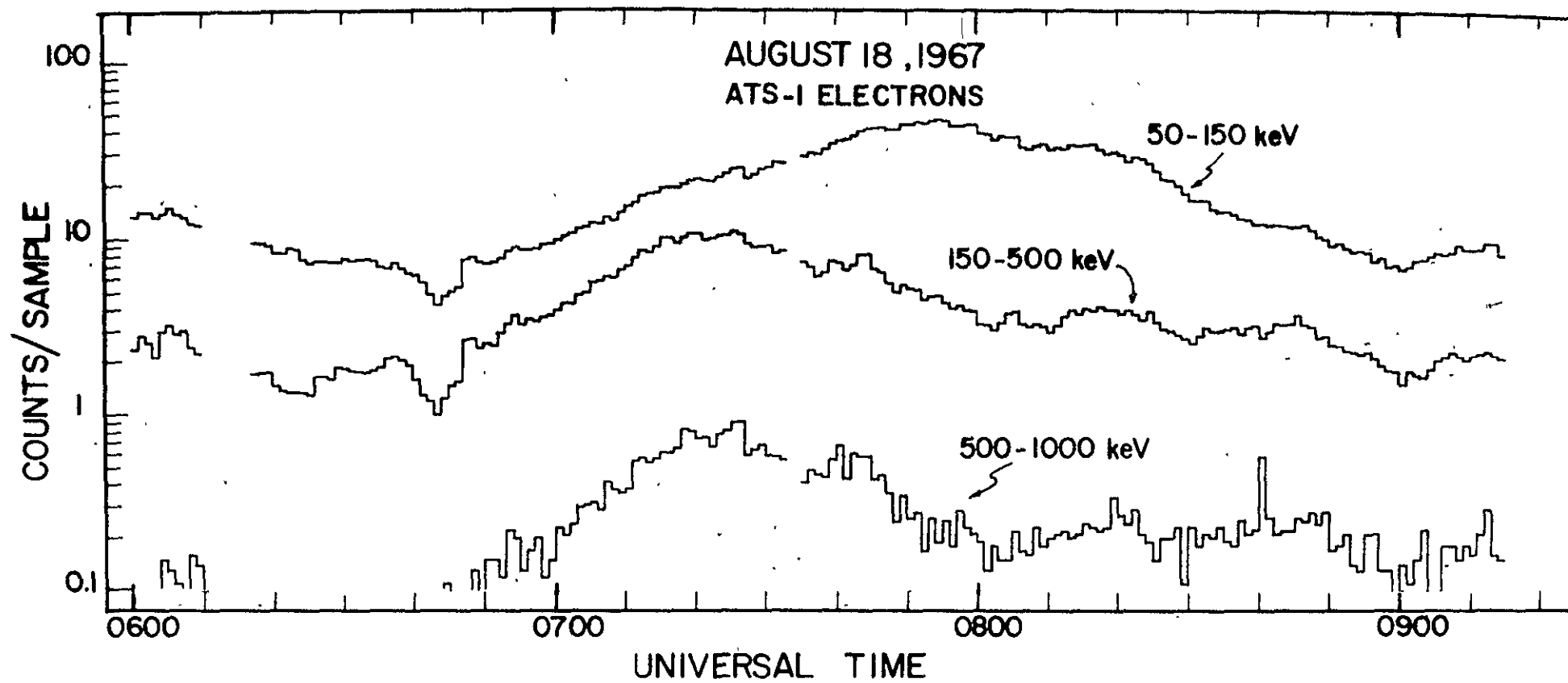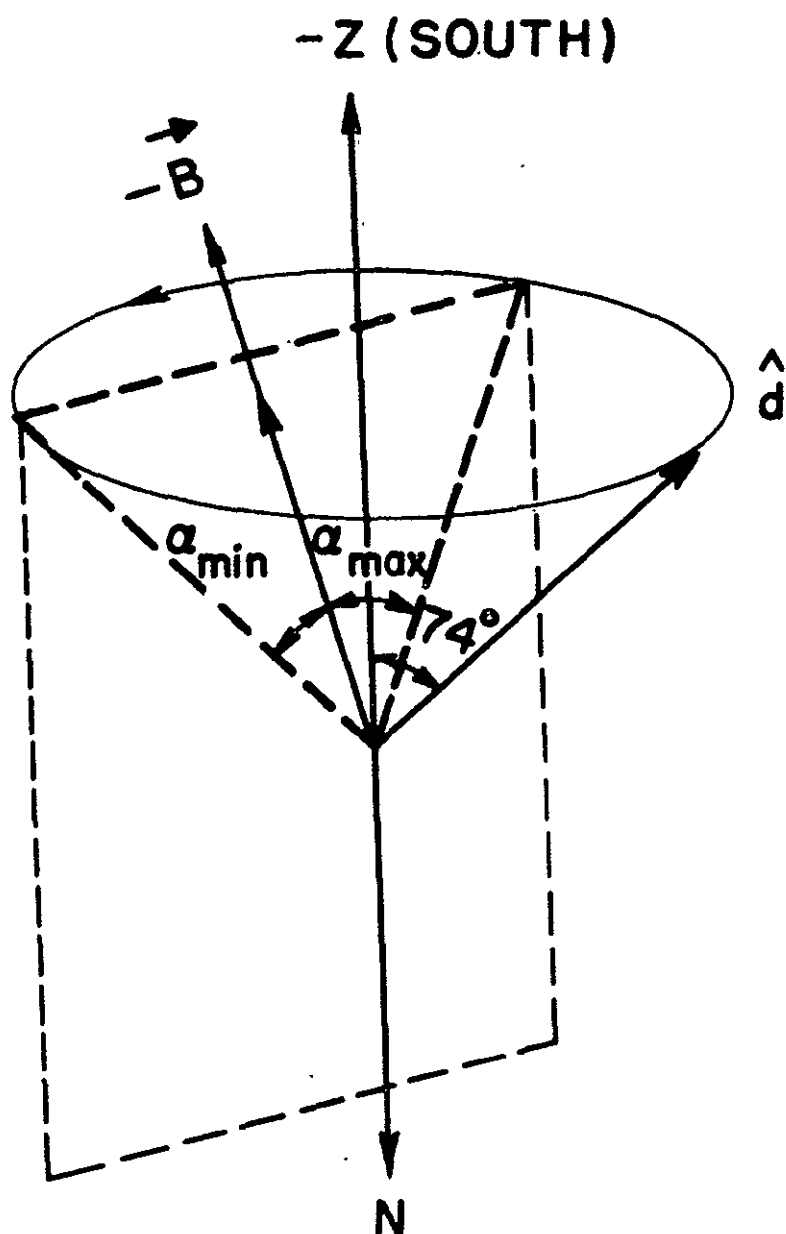
$\hat{Z}$ SPIN AXIS

$\vec{B}$ VECTOR MAGNETIC FIELD

$\hat{d}$ VECTOR ALONG DETECTOR AXIS

α_{min} MINIMUM PITCH−ANGLE SAMPLED

α_{max} MAXIMUM PITCH−ANGLE SAMPLED

Figure 17

Figure 18

APRIL 19, 1967
PITCH-ANGLE DISTRIBUTION
(150 - 500 keV)
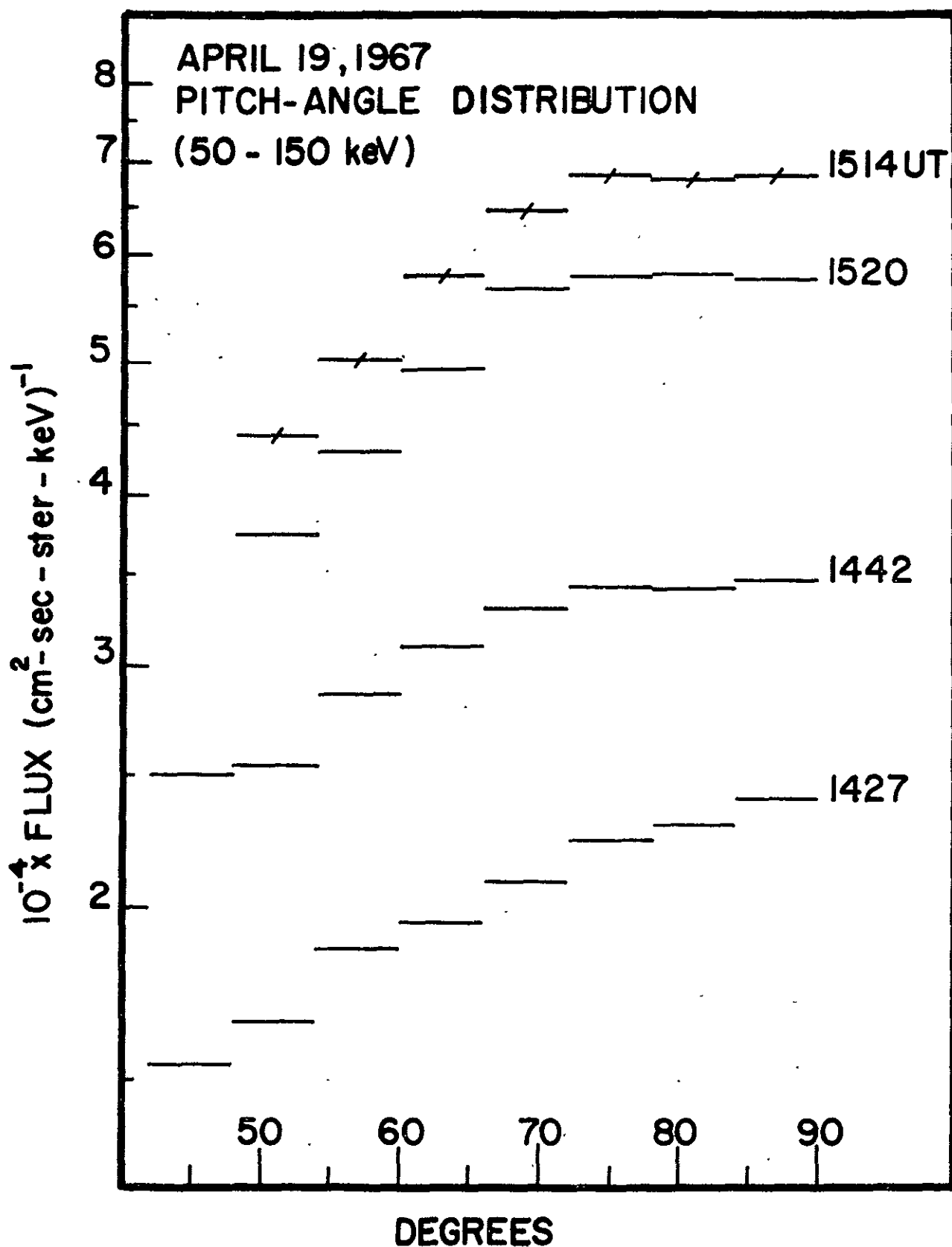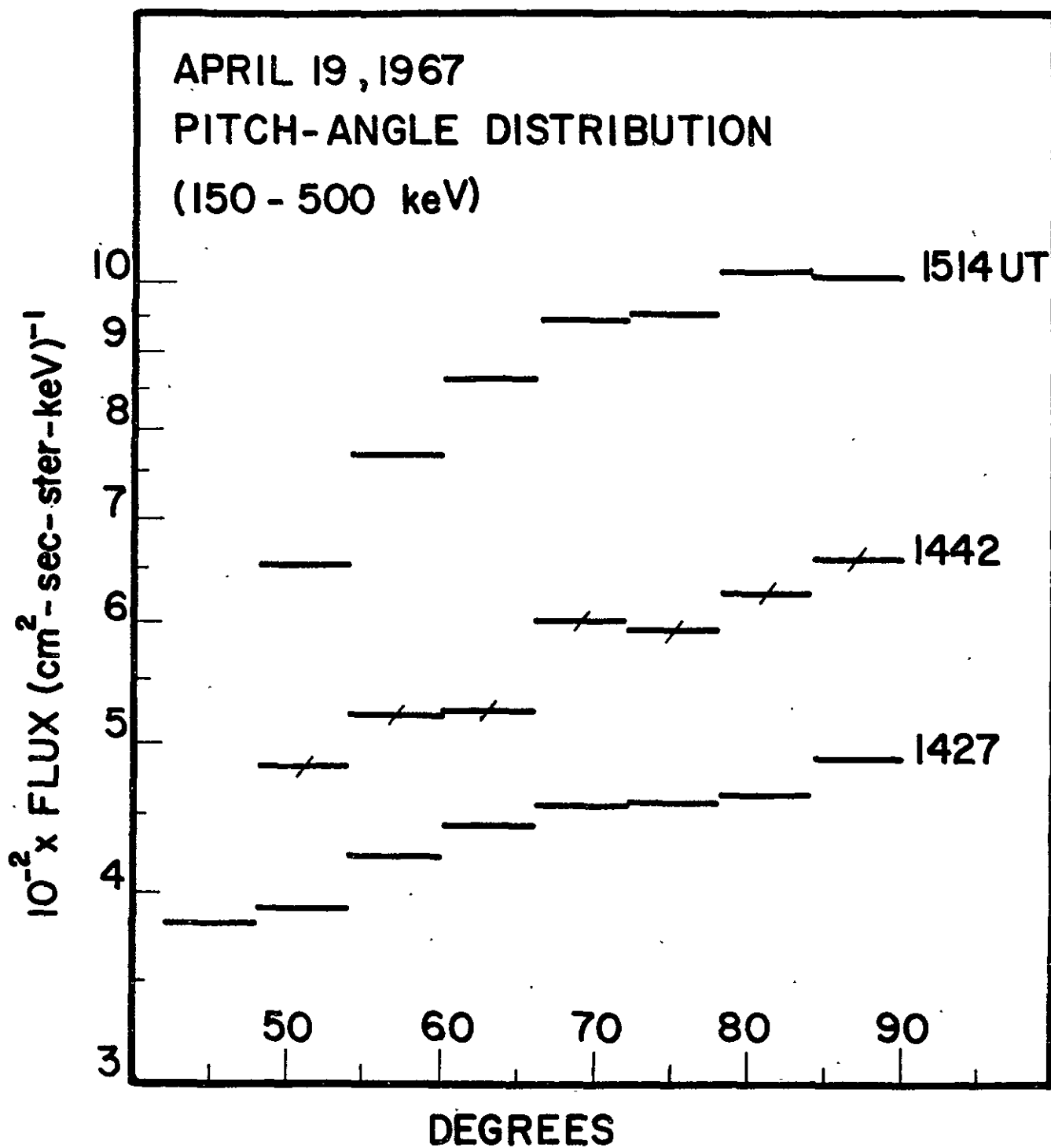
Figure 19

APRIL 19, 1967
PITCH-ANGLE DISTRIBUTION

Figure 20
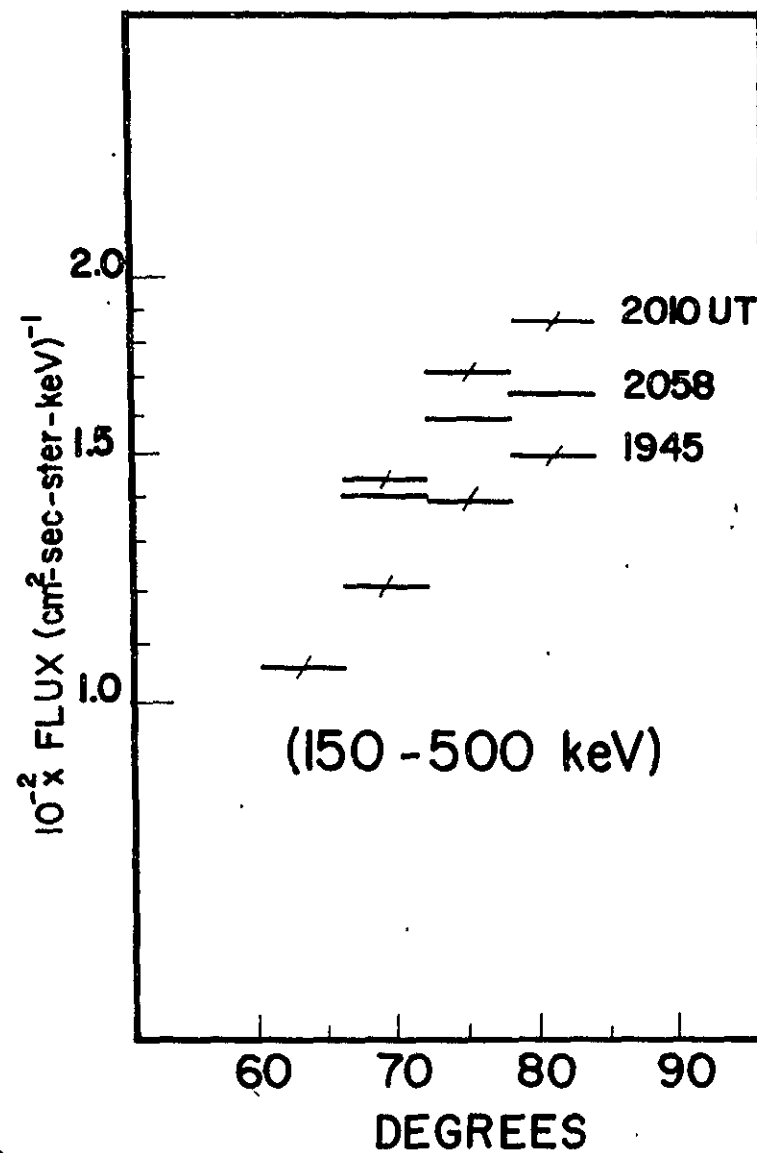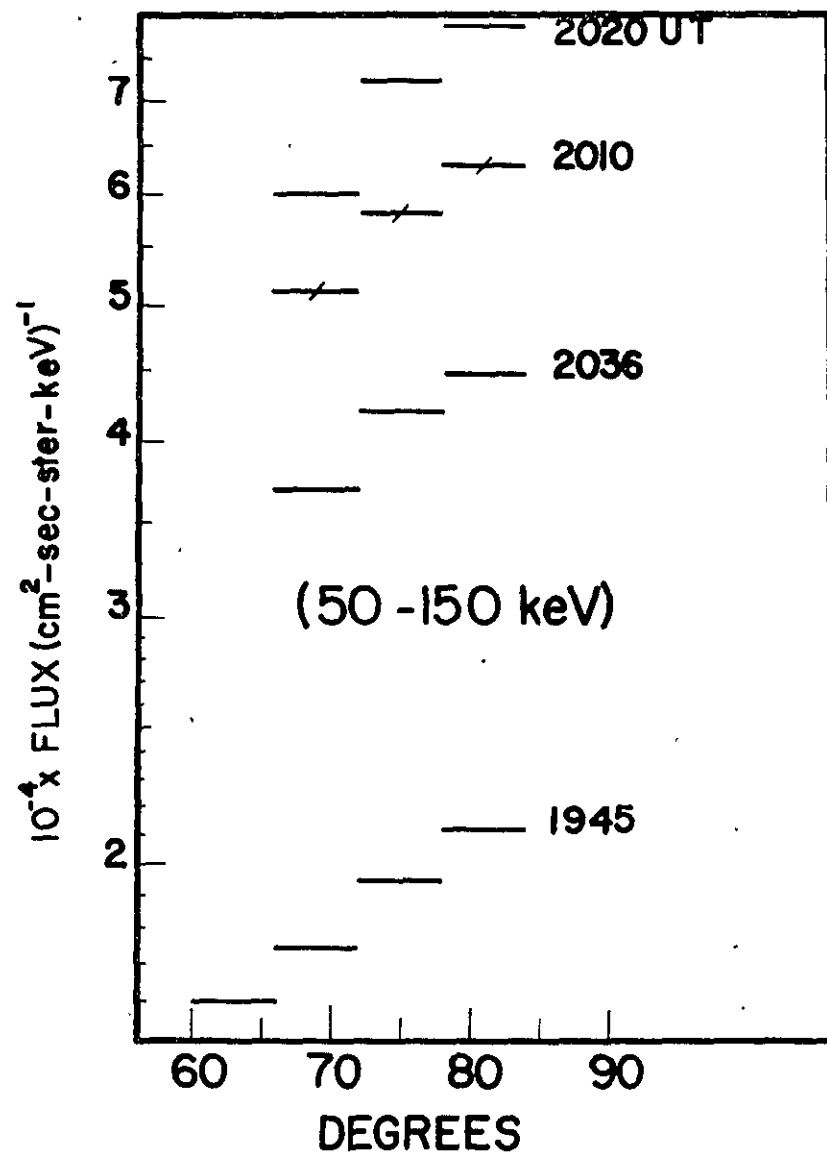
Figure 21

Figure 22

AUGUST II, 1967
PITCH-ANGLE DISTRIBUTION

(50-150 keV)

(150-500 keV)
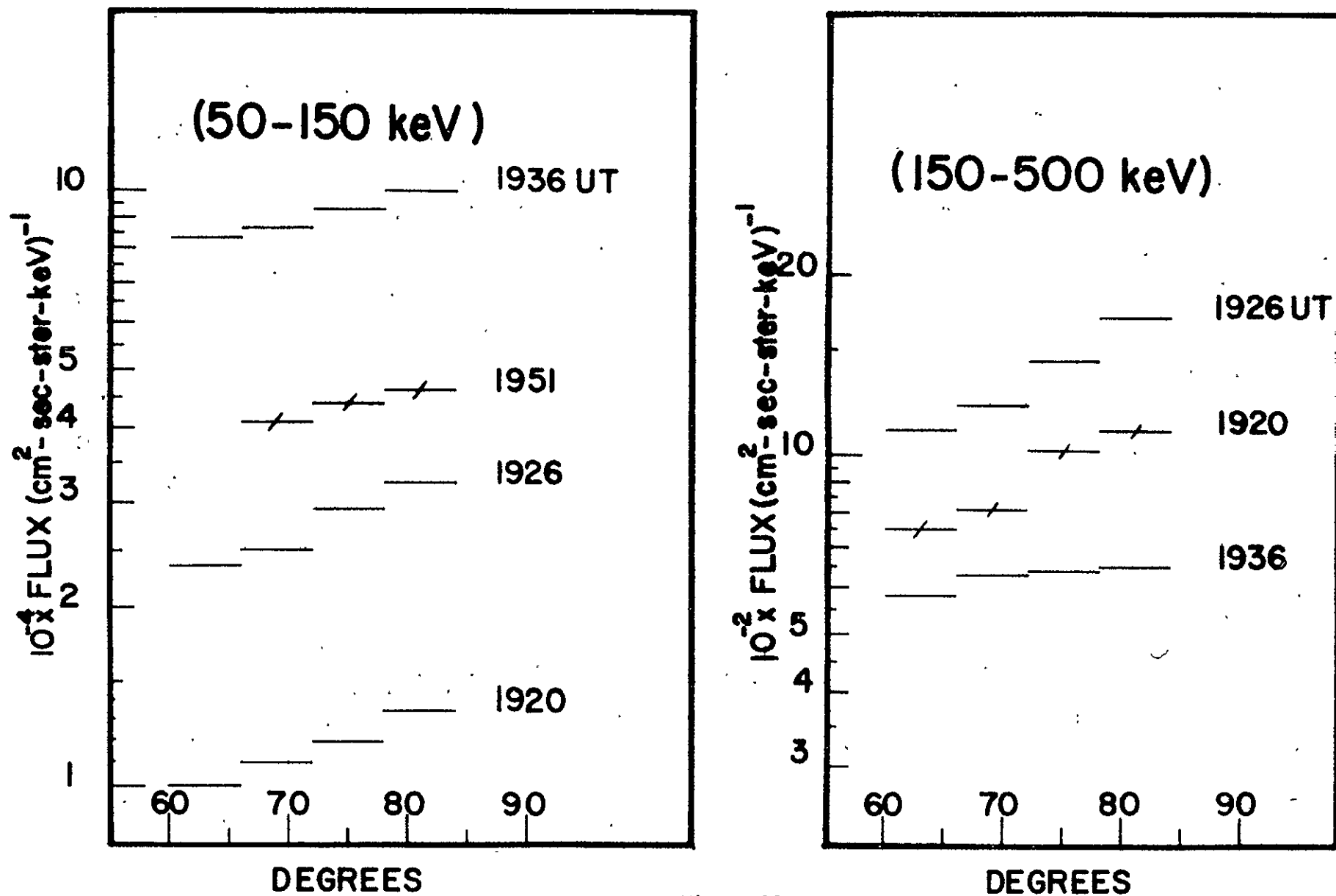
Figure 23

PITCH ANGLE DISTRIBUTION (AUG.11,1967)
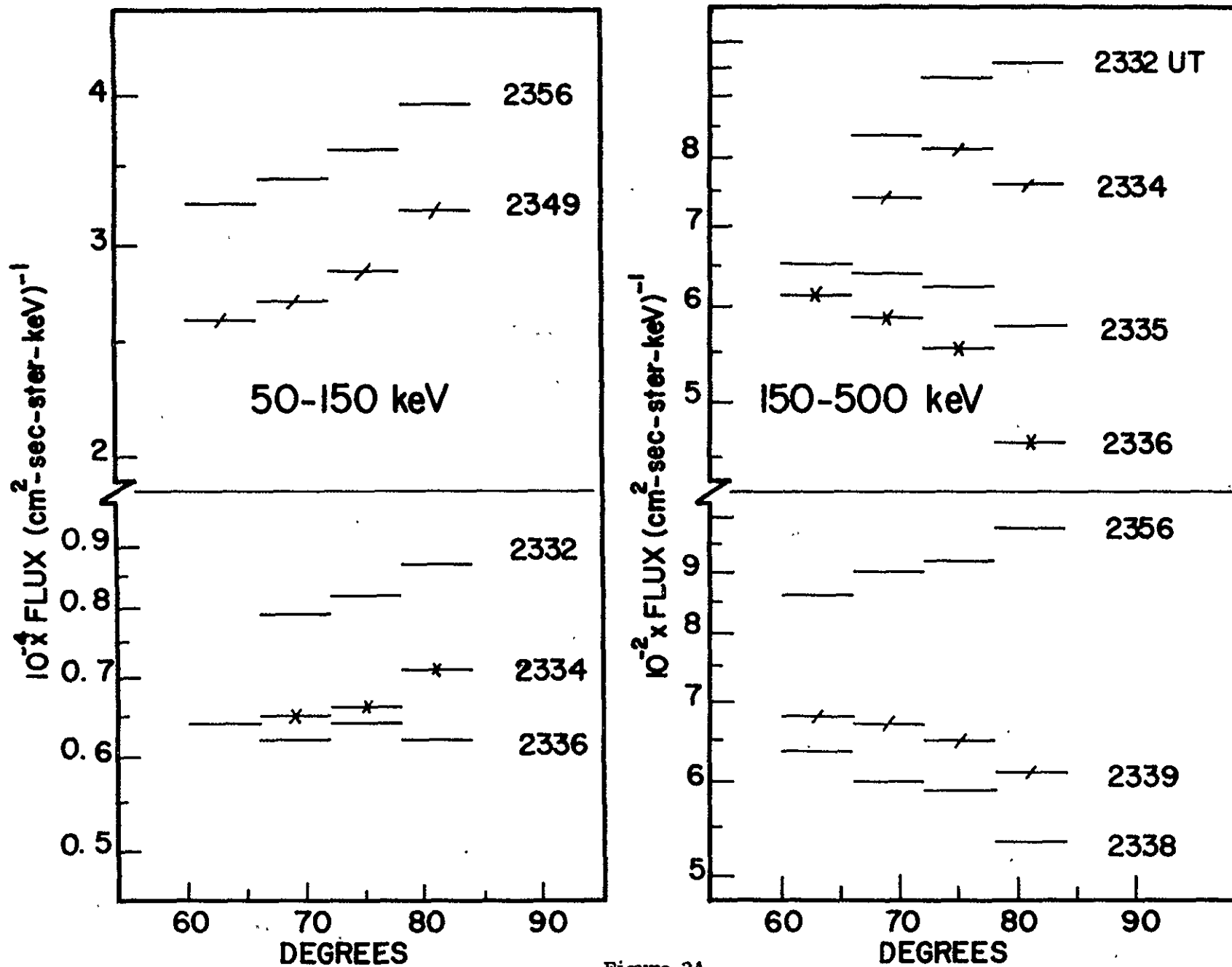
Figure 24

Figure 25

Figure 26

ATS-I ELECTRONS (150-500 keV, α = 57-90°)

APRIL 21, 1967

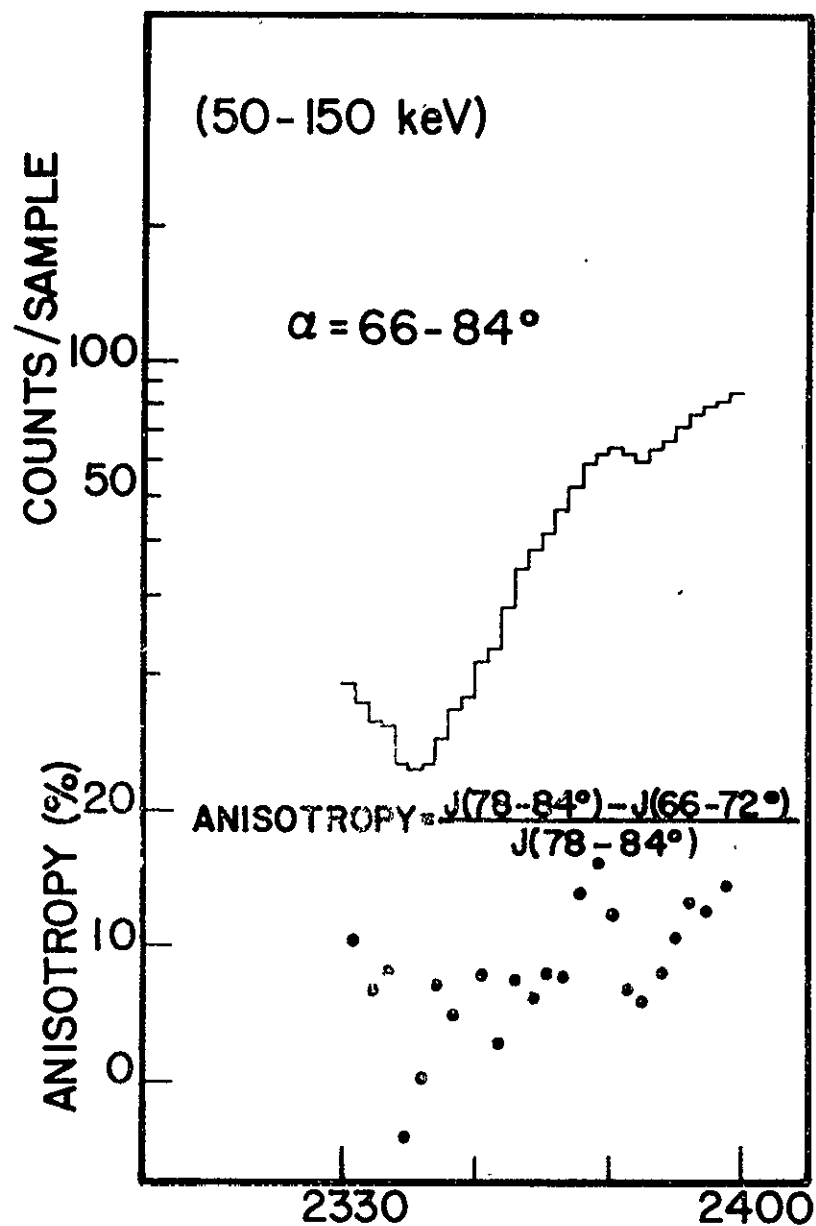$$\text{ANISOTROPY} = \frac{J(84-90°) - J(57-63°)}{J(84-90°)}$$
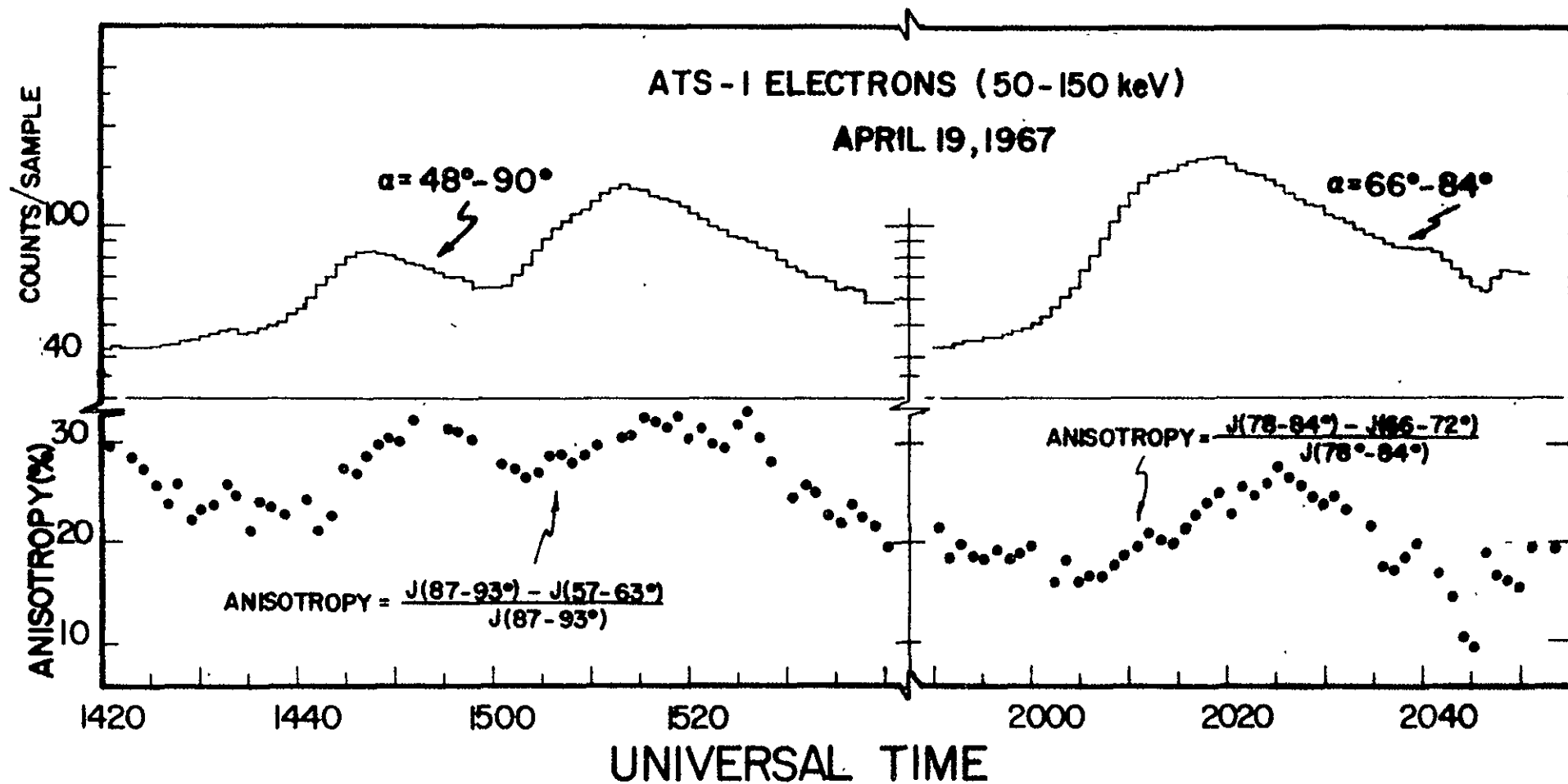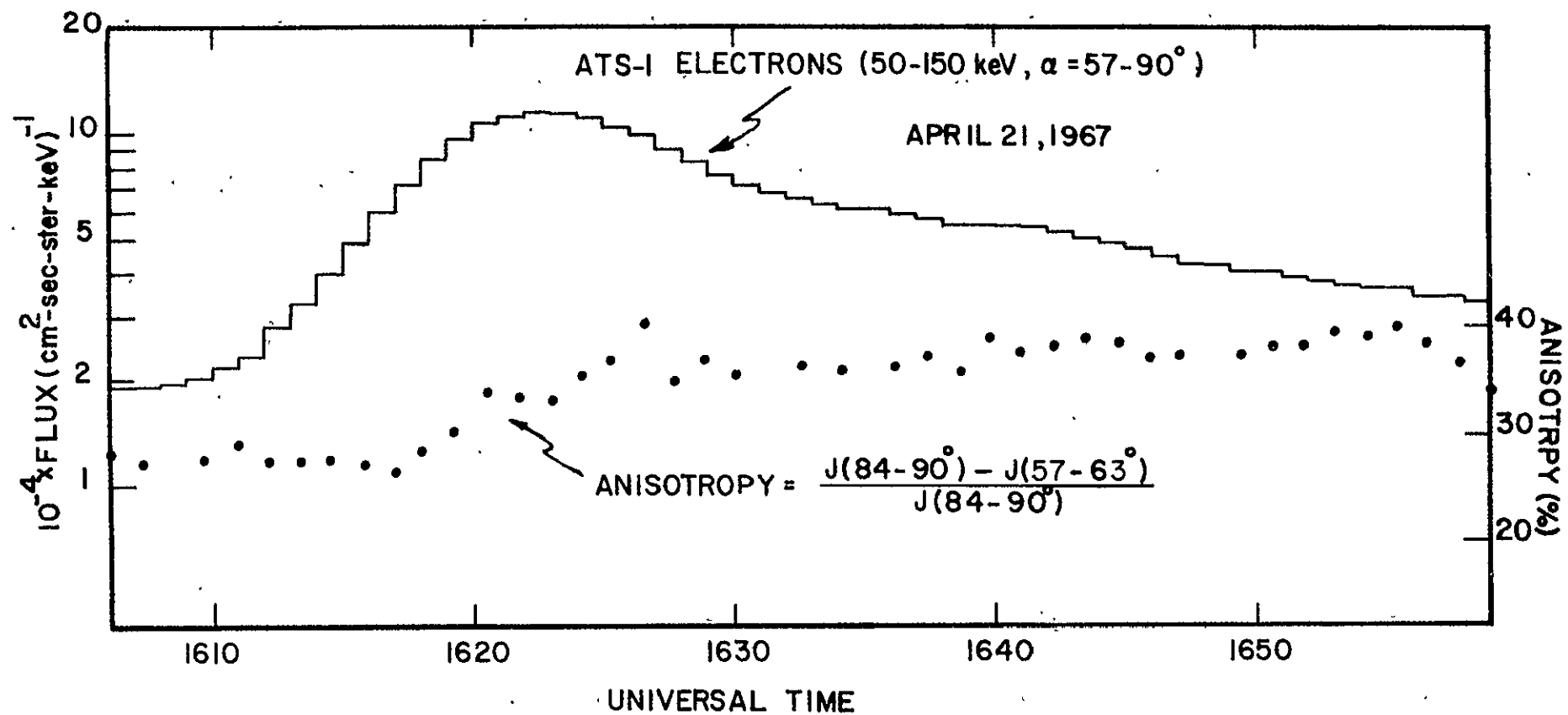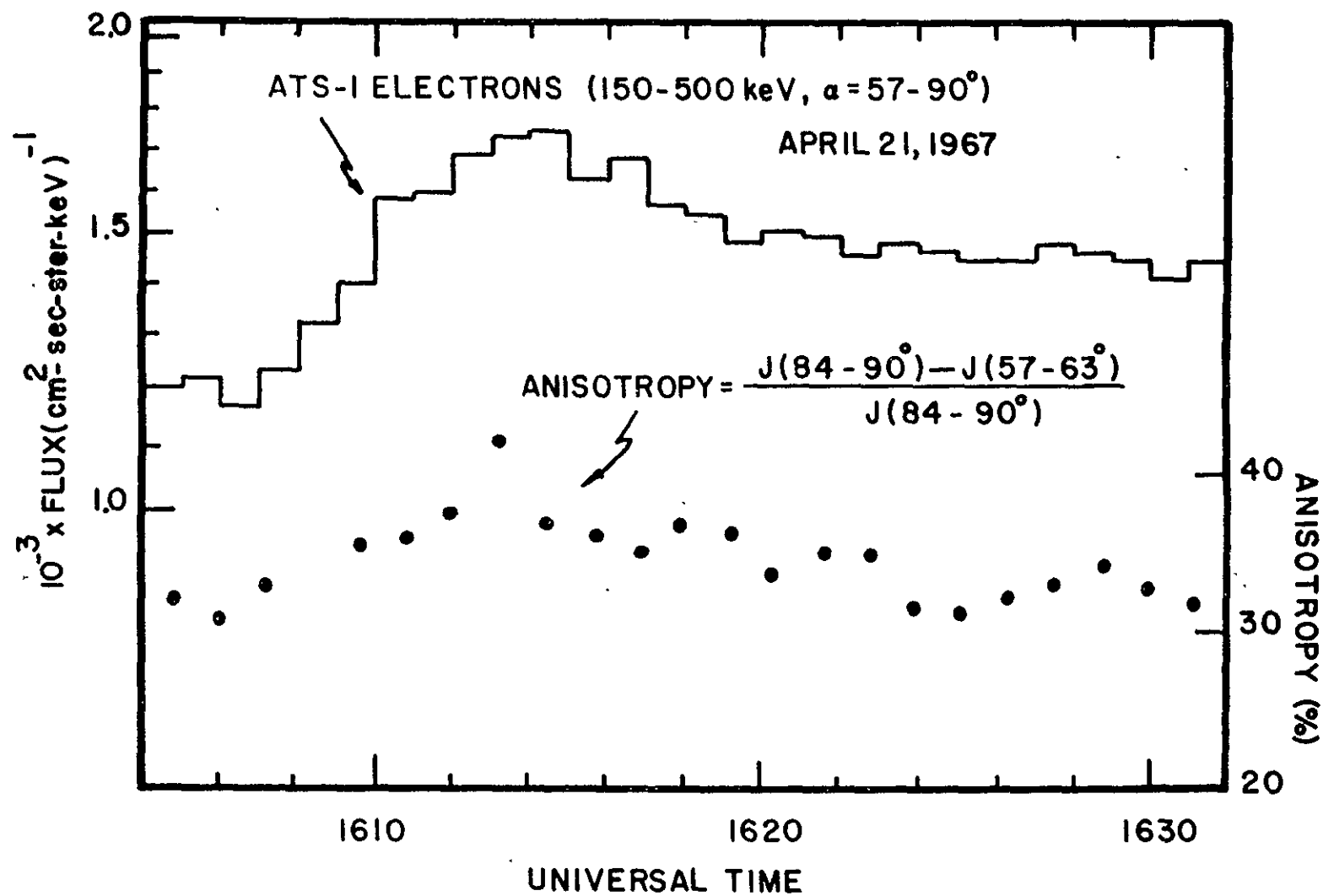
Figure 27

Figure 28

ATS-1 ELECTRONS (AUGUST 11, 1967)

Figure 29

Figure 30